NASA CR-165338
PWA-5594-141

NASA

ENERGY EFFICIENT ENGINE
LOW-PRESSURE TURBINE BOUNDARY LAYER PROGRAM
TECHNOLOGY REPORT

Prepared by

W. B. Gardner, Program Manager
Energy Efficient Engine Component
Development and Integration Program

UNITED TECHNOLOGIES CORPORATION
Pratt & Whitney Aircraft Group
Commercial Products Division

Prepared for

NATIONAL AERONAUTICS AND SPACE ADMINISTRATION
Lewis Research Center
Cleveland, Ohio 44135
Contract NAS3-20646

FOREWORD

The Energy Efficient Engine Component Development and Integration Program is being conducted under parallel National Aeronautics and Space Administration contracts to Pratt & Whitney Aircraft Group of United Technologies Corporation and General Electric Company. The overall project is under the direction of Mr. C. C. Ciepluch. Mr. John W. Schaefer is the NASA Assistant Project Manager for the Pratt & Whitney Aircraft effort under NASA Contract NAS3-20646, and Mr. Michael Vanco is the NASA Project Engineer responsible for the portion of the project described in this report. Mr. William B. Gardner is Manager of the Energy Efficient Engine project at Pratt & Whitney Aircraft Group. Dr. Om P. Sharma was the principal investigator for the effort.

TABLE OF CONTENTS

LIST OF ILLUSTRATIONS

LIST OF ILLUSTRATIONS (Continued)

LIST OF ILLUSTRATIONS (Continued)

LIST OF TABLES

SECTION 1.0

SUMMARY

This report presents results of a study conducted to investigate the development of boundary layers under the influence of velocity distributions simulating the suction sides of two state-of-the-art turbine airfoils. One velocity distribution represented a forward loaded airfoil ("squared-off" design) while the other represented an aft loaded airfoil ("aft-loaded" design).

These velocity distributions were simulated in a low-speed high-aspect-ratio wind tunnel specifically designed for boundary layer investigations. Detailed measurements of boundary layer mean velocity and turbulence intensity profiles were obtained for an inlet turbulence level of 2.4 percent and an exit Reynolds number of 8×10^5. Flush-mounted hot-film probes were used to identify the boundary layer transition regimes located in the adverse pressure gradient regions for both velocity distributions. Wall intermittency data showed good agreement with the correlation of Dhawan and Narasimha for the intermittency factor distribution in transitional flow regimes.

The boundary-layer mean velocity profile data from various axial stations were compared with predictions obtained from a differential boundary layer calculation method which used the McDonald-Fish turbulence model; agreement was good. The experimental data indicated that the squared-off velocity distribution generated a momentum loss thickness of about eight percent less than the aft-loaded distribution.

Data in the laminar boundary layer region showed a gradual increase in turbulence intensity in the streamwise direction. A hypothesis is proposed relating the increase of turbulence intensity to the onset of transition. The detailed data presented in this report are intended to be used to develop improved turbulence models suitable for application to turbine airfoil design.

Results are also reported for a parametric study conducted to assess the influence of turbulence level and Reynolds number on suction surface losses for the two airfoil designs; the above boundary layer solution procedure was used. This study indicated that the aft-loaded pressure distribution gives lower losses at higher Reynolds number, and the squared-off pressure distribution gives lower losses at lower Reynolds numbers. Therefore, an aft-loaded airfoil may be recommended for high-pressure turbines and earlier stages of low-pressure turbines and a squared-off airfoil for the later stages of low-pressure turbines.

SECTION 2.0

INTRODUCTION

The Low-Pressure Turbine Boundary Layer Program was an analytical and experimental investigation conducted under the Supporting Technology portion of the Energy Efficient Engine Program (Contract NAS3-20646), the objective of which is to develop and evaluate technology that will substantially reduce the fuel consumption of commericial aircraft engines and to demonstrate this technology in a research engine, the "Energy Efficient Engine". The purpose of the Boudary Layer Program was to investigate the possibility of further improving the efficiency of the low-pressure turbine by reducing airfoil profile losses. The program was conducted to ensure timely interaction with the low-pressure turbine component effort, as summarized in Figure 1.

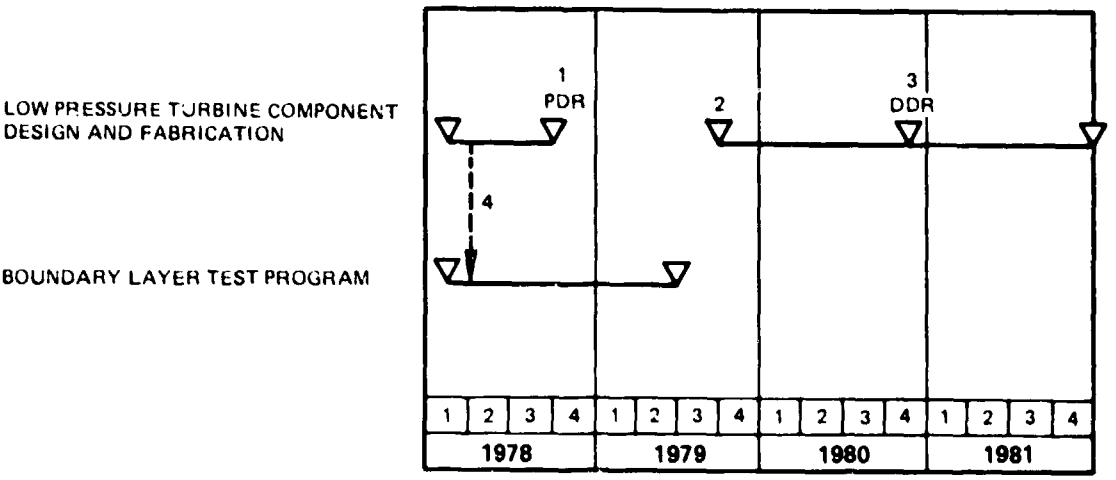

1 - COMPONENT PRELIMINARY DESIGN COMPLETED
2 - COMPONENT DETAILED DESIGN INITIATED
3 - COMPONENT DETAILED DESIGN COMPLETED
4 – AIRFOIL SELECTION CRITERIA PROVIDED TO TEST PROGRAM FROM COMPONENT PRELIMINARY DESIGN EFFORTS

Figure 1 Low-Pressure Turbine Boundary Layer Program Schedule

Profile losses are generated as a result of the development of boundary layers on the airfoil surfaces. For well designed turbine airfoils, 75 to 80 percent of the loss can be attributed to the boundary layer on the suction surface, making it the significant surface for investigation. Presently the most effective method of estimating this loss is to predict the boundary layer development by means of a boundary layer calculation procedure.

Several calculation procedures are available in the literature for estimating laminar and turbulent boundary layer development. However, boundary layers on turbine airfoils have large regions of transitional flows (refs. 1 and 2), and relatively few of the methods (refs. 3, 4, 5, 6, and 7) are capable of estimating the development of these boundary layers. In most existing procedures, concepts of turbulent boundary layers are extrapolated into transitional regimes in order to facilitate computation.

McDonald and Fish[3], using the turbulent kinetic energy transport equation with several assumptions about the structure of turbulence in transitional flows, were able to predict heat transfer data on turbine cascades. These assumptions were based on intuititive arguements and not on analytical formulation or experimental data. Arnal and Michel[4] and Wilcox[5] used a two equation turbulence model and Donaldson[6] used a five equation turbulence model for calculating transitional boundary layers. Several constants in these higher order turbulence models were selected to optimize computer calculations instead of modeling the physics of the transitional flow process. The lack of experimental data for transitional boundary layers has hindered proper evaluation of these models.

Intermittency factor is the only reliable feature of transitional flows that has been identified through the classical experimental investigations of references 8, 9, and 10. The variation of wall intermittency factor distribution was found to have a universal shape in transitional regions for boundary layer flows with a zero pressure gradient. However, none of the above turbulence models (refs. 3, 4, 5, and 6) utilize this information explicitly for calculating transitional flows. Forest[7] is the only author who utilized information about intermittency factor distribution, and he generalized it for boundary layers developing under the influence of pressure gradients. However, Forest had to use some intuitive arguments and empirical constants before hecould predict heat transfer data on turbine airfoils, and his predictions were no better than those obtained by McDonald and Fish[3]. No published data are available in open literature that would substantiate Forest's assumptions. Transition on turbine airfoils can occur either in accelerating or in diffusing flow fields, and data are needed to establish the behavior of the intermittency factor.

Current methods for calculating transitional boundary layers thus employ numerous assumptions that cannot be verified because of a lack of detailed experimental data. The objective of the present study was to experimentally assess the mean and turbulent velocity profiles developing under the influence of pressure gradients typical of state-of-the-art turbine airfoils. The resulting boundary layer data would provide unique insight into the processes governing the onset of transition for developing boundary layers.

Two velocity distributions were selected representing candidate airfoil designs for the fourth blade mean section of the low-pressure turbine. Simulation of boundary layers for the suction surfaces of these two airfoils was obtained in a boundary layer tunnel by contouring the wall opposite a flat test plate.

Detailed measurements were obtained for a constant inlet turbulence level (Tu = 2.4%) and an approximately constant Reynolds number based on exit velocity and test section length ($Re_S = 8 \times 10^5$).

The resulting data, describing laminar, transitional, and turbulent regimes of each boundary layer, were compared with predictions by utilizing the turbulence model of McDonald and Fish[3]. The experimental results provide a data base for other investigators to evaluate existing turbulence models or develop new models.

The design of the test sections simulating the suction surfaces is presented for both the squared-off and aft-loaded airfoils.

The experimental work was conducted in a low-speed, high aspect ratio, recirculating type of boundary layer tunnel. The Reynolds numbers (based on exit velocity and test section length) of the two tests were 7.86×10^5 and 8.14×10^5 for the aft-loaded and squared-off configurations, respectively. Turbulence generating grids upstream of the contraction cone in the wind tunnel were used to obtain a free-stream turbulence level of about 2.4 percent at inlet to the test section. The boundary layer started from the leading edge stagnation point as a laminar layer and became turbulent in the diffusing section of the velocity distribution after passing through transitional region. The test plate was instrumented with flush-mounted hot-film probes to identify the state of the boundary layer. Experimental test facility, probes, and data acquisition equipment and procedure are described.

Extensive measurements were made throughout the test section at midspan for two different free-stream velocity distribution shapes. The measurements consisted of wall static pressure, wall intermittency factor distribition, boundary layers mean velocity, and turbulent intensity profiles. Data reduction procedures and methods of measurements are reported.

Comparisons of experimental data with theoretical predictions and empirical correlations are presented. Measured turbulent velocity profiles are compared with the Coles[11] profiles. Integral parameters calculated from the mean velocity profile data are compared with predictions from a differential type of boundary layer solution procedure that uses the McDonald-Fish turbulence model for transitional and turbulent boundary layer calculations. Momentum thichnesses in the exit plane of the test section for the two tests conducted are compared in order to establish the loss behavior of one pressure distribution relative to the other.

The boundary layer solution procedure was then used to calculate boundary layer development on the suction surfaces of the two airfoils for a range of Reynolds number and turbulence levels in order to establish the loss behavior of the suction surfaces of the two airfoils in flight condition.

Conclusions from the test and recommendations for the design of low loss airfoils are also presented.

SECTION 3.0

DESIGN AND ANALYSIS

The objective of the design and analysis effort was to select flow characteristics typical of those found on the suction surface of candidate low-pressure turbine airfoils and to design test sections that accurately simulate those flows. An understanding of boundary layer characteristics within the flow field is an important adjunct to this process.

3.1 BOUNDARY LAYER DEVELOPMENT

The airfoil profile loss is the sum of losses due to the boundary layer on the pressure and suction surfaces of the airfoil. The velocity gradient on the pressure surface is always of an accelerating nature and boundary layers in accelerating flows generate much lower losses than in zero velocity gradients or diffusing flows, thus the boundary layer on the pressure surface is responsible for only about 15 to 20 percent of the total profile loss of an airfoil. The remainder of the loss is due to the boundary layer on the suction surface.

The distribution of wall static pressure on the suction surface of an airfoil shows flow acceleration from the leading edge stagnation point to minimum static pressure near the throat of the cascade and flow diffusion in the rear end of the airfoil (Figure 2). The growth of loss due to the boundary on such airfoils is dominated by the location of the onset of transition, as shown in Figure 2. Three sets of calculated momentum loss thickness growth are shown in this figure. The calculations were obtained by using Stan-5 boundary layer calculation method and McDonald-Fish turbulence model. Three sets of cacula-tions were obtained for three different inlet free-stream turbulence levels at an inlet Mach number of about 0.33, a total temperature of about 622^{o}R, and a total pressure of about one and one half atmosphere.

The interesting point about Figure 2 is that as the turbulence level is increased from 3.5 percent to 7 percent and then to 10 percent, the location of the onset of transition moves towards the leading edge of the airfoil, which in turn results in higher momentum loss thickness in the trailing edge of the airfoil. And as the turbulence level is reduced from 10 percent to 7 percent and then to 3.5 percent, the onset of transition moves towards the throat of the airfoil, and momentum loss thicknesses at the trailing edge of the airfoil reduce progressively.

The high turbulence curve (10%) in Figure 2 shows the boundary layer to be fully turbulent over most of the airfoil. Minimum loss at the trailing edge is given by 3.5 percent turbulence level (solid line in Figure 2). If the turbulence level were further reduced, transition would not occur and the boundary layer would separate, which should result in increased losses. Thus, minimum losses for an airfoil occur when the transition point is very near the throat of the airfoil. This figure indicates that if a method were to be developed that inhibits the onset of transtion up to the throat location, the airfoil would give minimum loss.

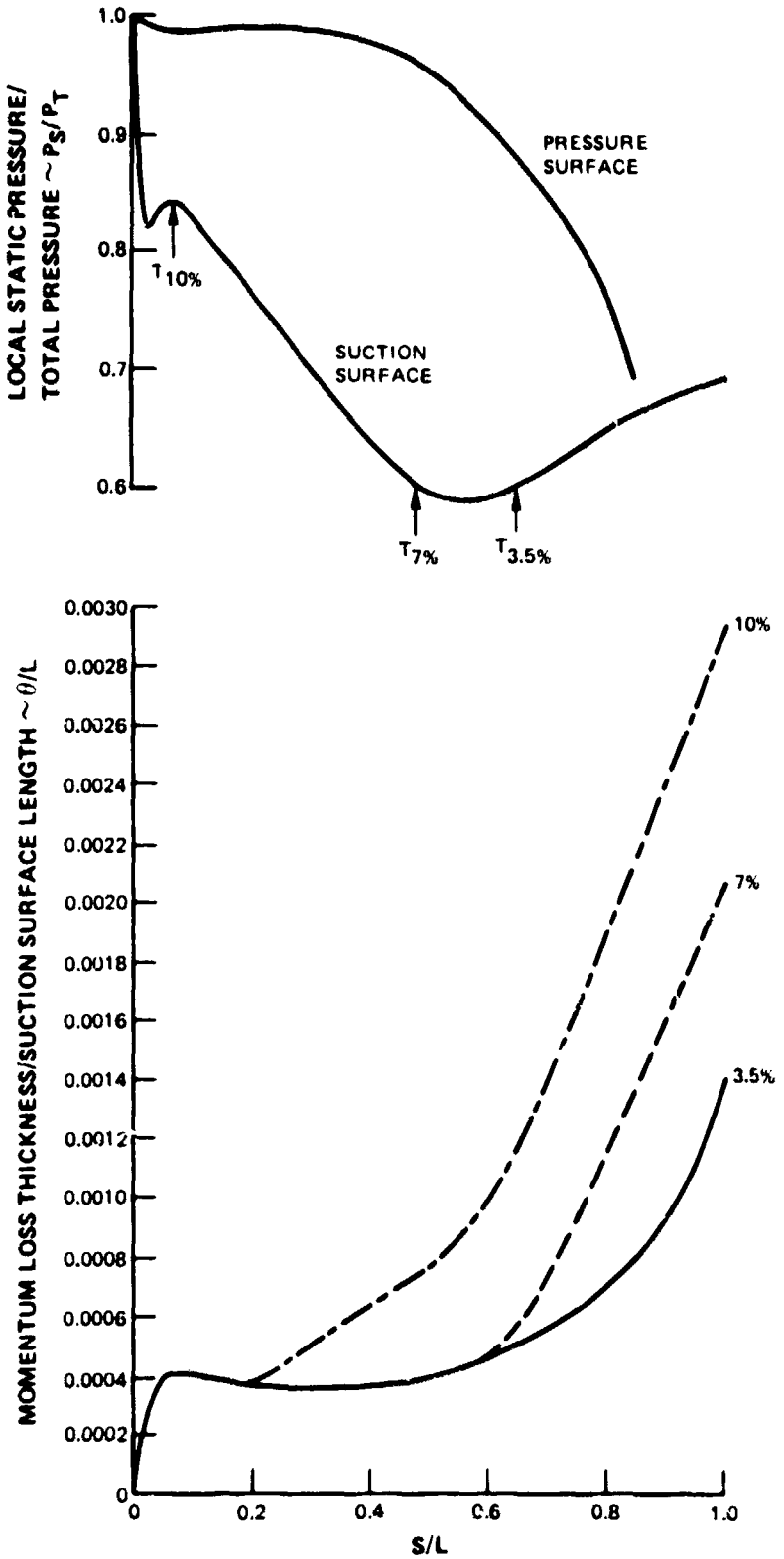

Figure 2 Ratios of Momentum Loss Thickness to Suction Surface Length and Local Static Pressure to Total Pressure as Functions Percent Suction Surface Length

A number of parameters influence the location of the onset of transition; the following are among the most important:

- o Airfoil surface curvature
- o Free-stream turbulence intensity
- o Reynolds number
- o Free-stream velocity (pressure) distribution shape, etc.

Suction surfaces of turbine airfoils usually have convex curvatures, which Liepmann[12] has shown have little effect on the onset of transition.

Although turbulence levels in turbines are known to be very high (above 4%), definite measurements have not been made in real turbines. Since high turbulence levels are difficult to generate in wind tunnels without distorting the mean flowfield, detailed boundary layer measurements for specific turbulence levels would allow one of the reference turbulence models (3, 5, 6, or 7) to be used to extrapolate the information for realistic turbine operating conditions. The reference 3 model (McDonald-Fish) was employed for this program.

For a given velocity triangle in a turbine row, Reynolds number is almost fixed, leaving the shape of the free-stream velocity distribution to be investigated. The Program tests were conducted to study the effect of this parameter on the boundary layer development, the main objectives being:

1. To provide a comparison of the boundary layer momentum loss thickness (hence, profile loss) on the simulated suction surface of a low-pressure turbine airfoil of the Energy Efficient Engine design (aft loaded) and an equivalent airfoil with a squared-off pressure distribution.

2. To calibrate the profile-loss prediction method for the Energy Efficient Engine airfoil--which is a differential type of boundary layer solution procedure--with the simulated boundary layer data and then conduct a parametric study to predict the profile loss behavior of squared-off and aft-loaded airfoils. The study would cover takeoff and cruise conditions (i.e., high and low Reynolds numbers).

3. To provide detailed data of boundary-layer mean and turbulence velocity profile in order to permit the turbulence model of the boundary layer solution procedure to be checked in detail.

3.2 AFT-LOADED/SQUARED-OFF DESIGNS

In designing for low losses, Pratt & Whittney Aircraft usually designs the suction side of the airfoil to have high accelerating pressure gradients up to the minimum pressure point to ensure laminar flow to that point, the diffusion occurring in the latter part of the airfoil. This is the aft-loaded design. Apart from the advantage of low losses, these airfoils can operate favorably at high positive and negative incidences.

An alternate airfoil design used in the industry provides a steep acceleration on an earlier point of the airfoil, holds the velocity constant in the middle of the airfoil, and diffuses in the latter part of the suction surface. This is the squared-off design. Airfoils of this design have lower airfoil-surface Mach numbers and lower velocity diffusion and, under favorable conditions, have the potential to give lower loss than the aft-loaded airfoils. However, if one assumes transition to occur at the end of the acceleration region, because of a high free-stream turbulence level, the squared-off airfoils will have a larger region of fully turbulent flow than the aft-loaded airfoils; hence, one would expect higher profile losses.

Two velocity distributions were selected that represented candidate designs of the fourth blade mean section of the low-pressure turbine component. The two airfoil shapes and the predicted pressure distribution associated with each geometry are shown in Figure 3.

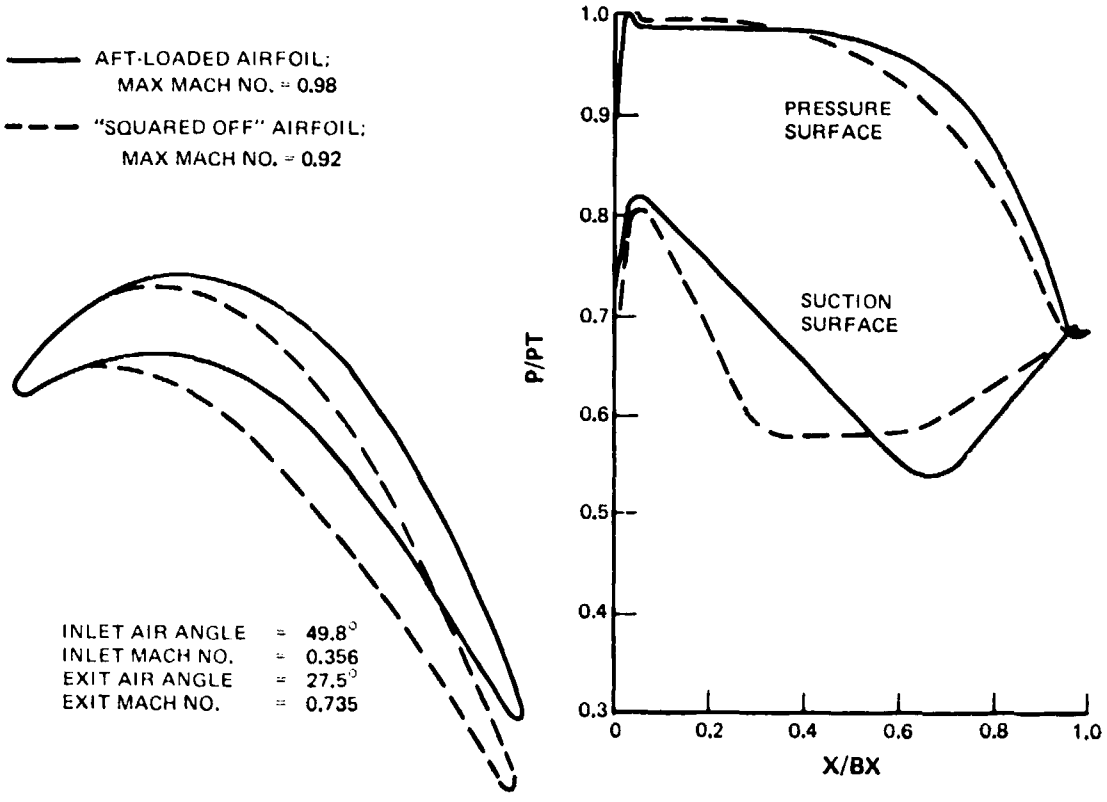

Figure 3 Two State-of-the-Art Turbine Airfoil Profiles and the Associated Surface Static Pressure Distributions.

3.3 AIRFOIL SUCTION SURFACE SUMULATION

Measurements of the boundary layer on a full-scale cascade are almost impossible to obtain because boundary layers are too thin to be measured by state-of-the-art instrumentation. To obtain measurable boundary layers on an airfoil, the airfoil would have to be about three feet long, and no cascade facility was available to the program that would accept such a size. Also, detailed measurements of airfoil boundary layers in large cascades require very sophisticated instrumentation and even then the accuracy of the measurements is open to question (reference 13). To meet test requirements, the desired pressure distributions were simulated on a flat plate in a boundary layer tunnel. The prescribed pressure distribution was imposed on the flat wall test plate by contouring the opposite wall.

Test sections were designed for Reynolds number of about 8.0×10^5 (based on test plate length and exit velocity), which matched the cascade test being conducted for the Energy Efficient Engine, Low-Pressure Turbine Technology Program, where both airfoil designs are being tested full scale in order to provide loss comparisons. The contoured wall was designed using the Casper et al [2] potential flow procedure for a cascade. The flat surface was considered to be the suction surface, and the contoured wall was changed until proper velocity distribution on the test plate was obtained. The viscous blockage on the walls was taken into consideration through the use of a boundary layer calculation method. The required velocity distribution through the test section was obtained by maintaining a Reynolds number similarity between the test section and the airfoil under consideration.

The geometries of the two test sections designed in the above manner and the designed pressure distributions for the two sections are shown in Figure 4, and coordinates for the test sections (contoured walls) are given in Appendix A.

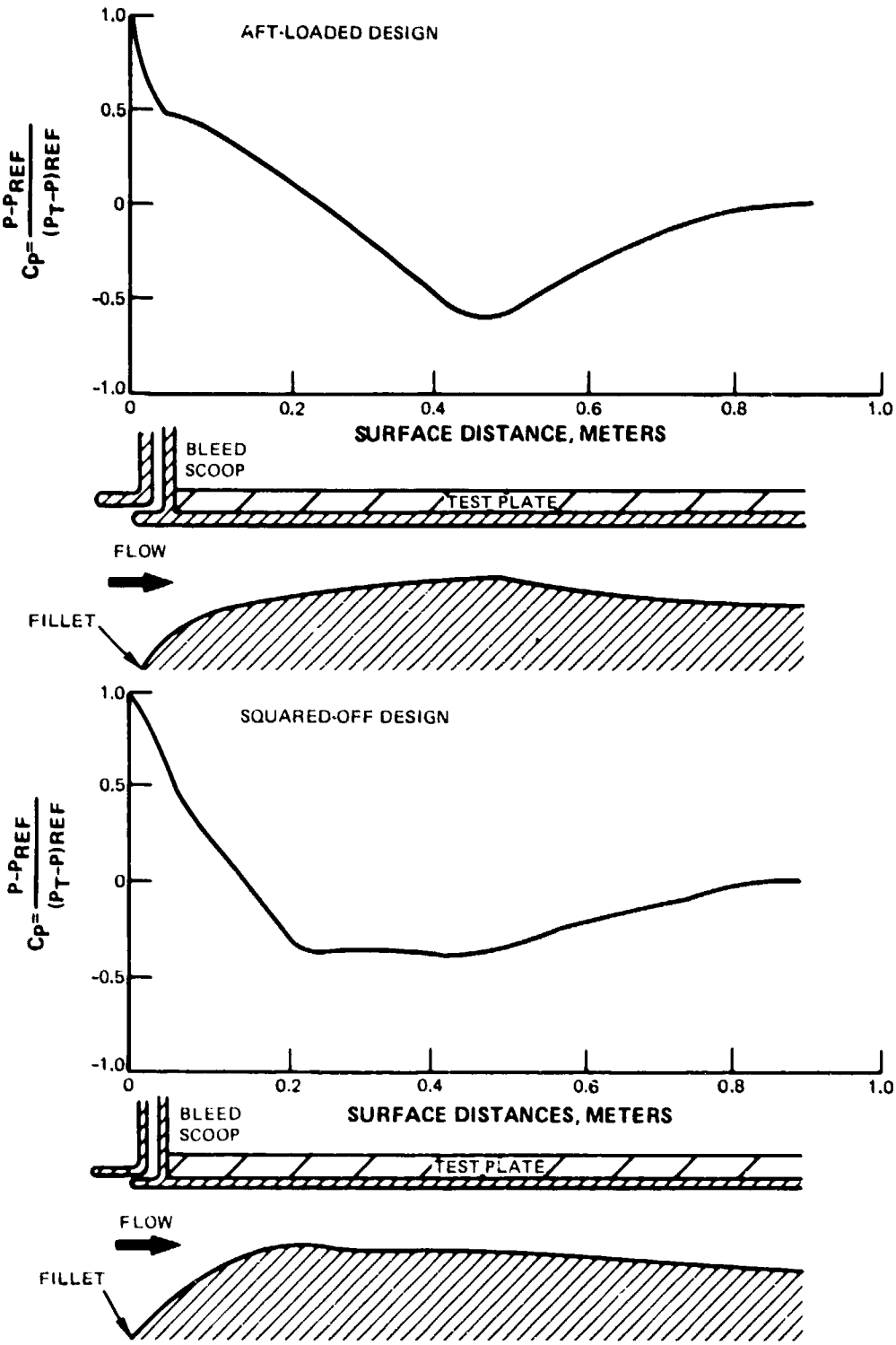

Figure 4 Test Section Geometries and Simulated Pressure Distributions for the Aft-Loaded and Squared-Off Airfoils

SECTION 4.0

TEST FACILITIES

4.1 WIND TUNNEL

The program tests were conducted in a low-speed boundary-layer wind tunnel at the United Technologies Research Center. This tunnel, which can operate at a constant air temperature over a wide range of flow speeds and turbulence levels, was designed for fundamental studies of two-dimensional, incompressible boundary layers. A schematic of the wind tunnel is shown in Figure 5.

The tunnel air velocity was controlled through a combination of variable-speed drives to the blower and adjustable inlet-guide vanes. Several devices located in the plenum were used to remove nonuniformity from the flow: a series of perforated baffles that attenuated gross irregularities in the blower exit flow, perforated plates, a honeycomb, and a series of eight screens. Turbulence generating grids that could be installed downstream of the screens were available to generate the turbulence intensity.

A nozzle downstream of the plenum accelerated the flow to 2.8 times the velocity in the plenum. At the exit plane of the nozzle, a free-stream turbulence level, $\sqrt{(u^2)}/U$ inlet, of 0.024 was measured. The total pressure coefficient measured at the exit plane of the nozzle was found to be within one percent of the reference condition (exit dynamic head) throughout the core flow.

The exit flow from the test section was diffused in a two-stage, variable-angle diffuser. A filter and a liquid-chilled heat exchanger followed the diffuser. The flow temperature was stabilized at approximately 295K. The test section was immediately down stream of the nozzle.

4.1.1 Test Section

The test section, located between the nozzle and diffuser, was 0.86 m wide and 2.44 m long and consisted of a flat test plate, a contoured wall, and two side walls. The test plate was equipped with 147 static-pressure taps and 187 holes for flush-mounted, hot-film probes. The length of the test plate for the present investigation was 0.915 m.

The inlet boundary layer was removed by means of a bleed scoop at the leading edge of the test plate, as shown in Figure 6. The flow through the bleed scoop was controlled by perforated plates and a valve. The flow was adjusted to have a slightly negative angle of attack at the second scoop in order to ensure a favorable pressure gradient along the leading edge of the test plate.

The wall opposite the test plate was contoured to generate required pressure distributions on the test plate. Two different contoured walls were used: one for the squared-off pressure distribution and one for the aft-loaded distribution. A number of holes was drilled in the contoured walls to insert the hot-film probes for boundary layer velocity profile measurements.

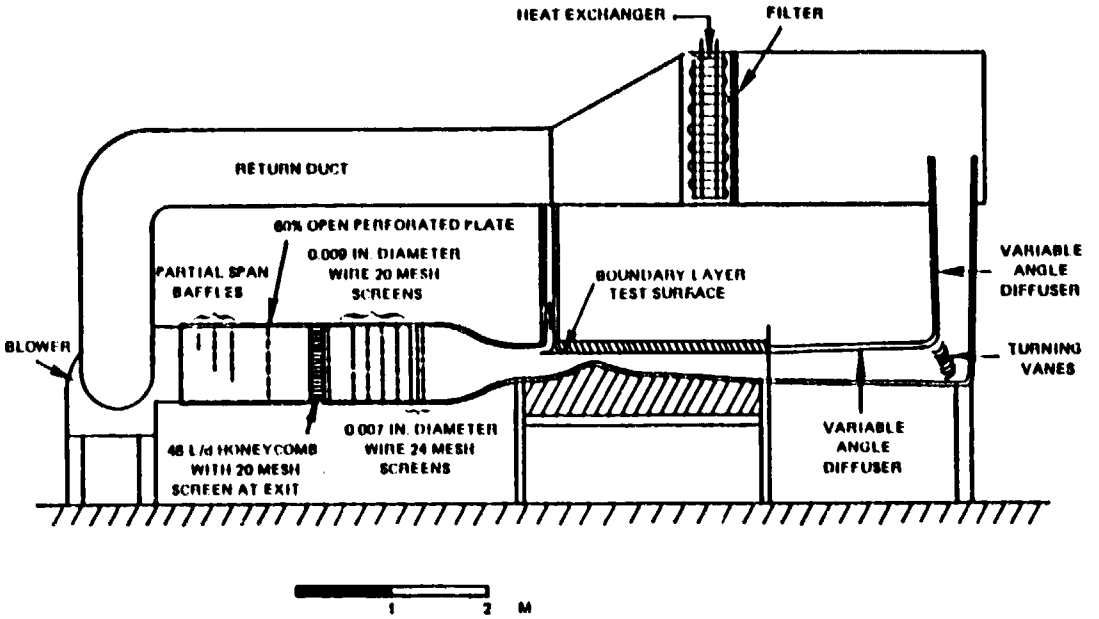

Figure 5 Boundary Layer Wind Tunnel Used in Low-Pressure Turbine Boundary Layer Program

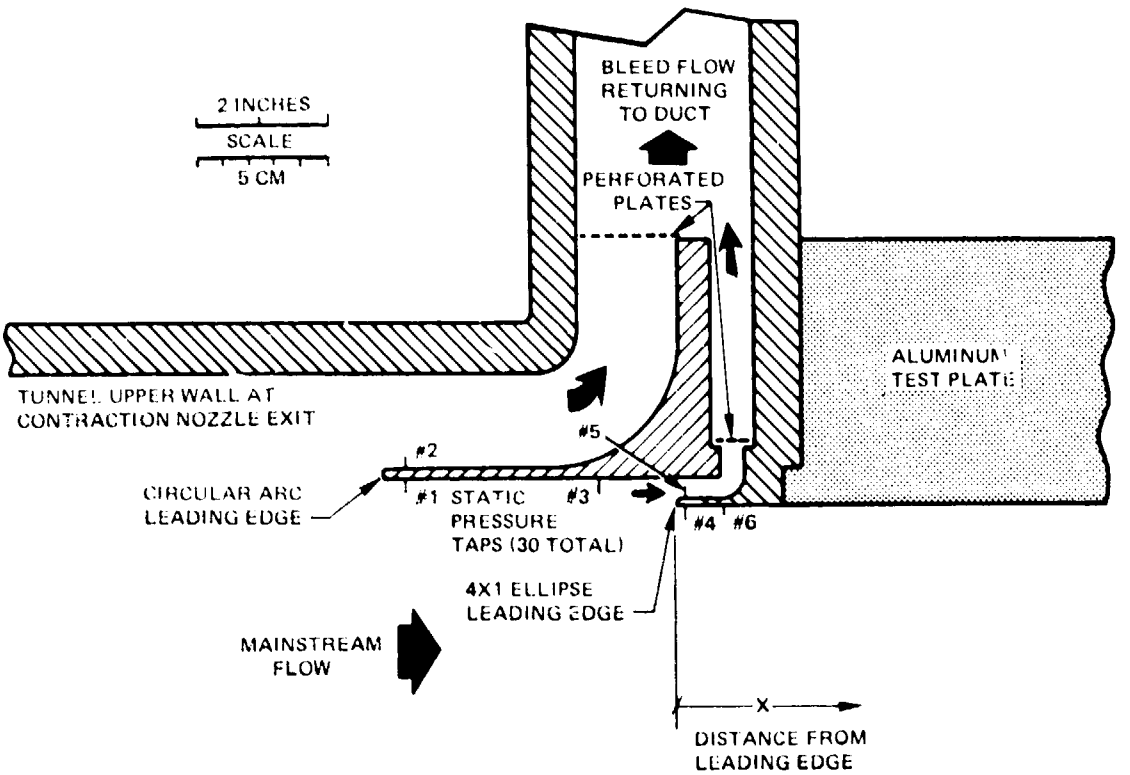

Figure 6 Boundary Layer Bleed Scoop (With 30 Static Pressure Taps, No. 1 to No.6)

The side walls were constructed of clear plexiglass to permit flow visualization and facilitate the positioning of probes.

To determine the relative magnitude of losses associated with the two turbine airfoil designs, detailed measurements were obtained of the mean and turbulence velocity profiles for the two test configurations. In principle, one mean velocity profile at the exit of each test section will give the relative magnitude of the loss associated with the two shapes of pressure distribution, but exit velocity profile will be insufficient to provide enough information about the detailed mechanisms involved in generation of losses through the test section. Thus, it was decided to obtain detailed measurements of boundary layer mean and turbulence quantities at predetermined locations for each configuration.

4.2 INSTRUMENTATION

4.2.1 Wall Static Pressure

Wall static pressure was measured at 58 locations on the test plate, see Figure 7. The transducer used to record the static pressure was calibrated using a ten-inch water micromanometer.

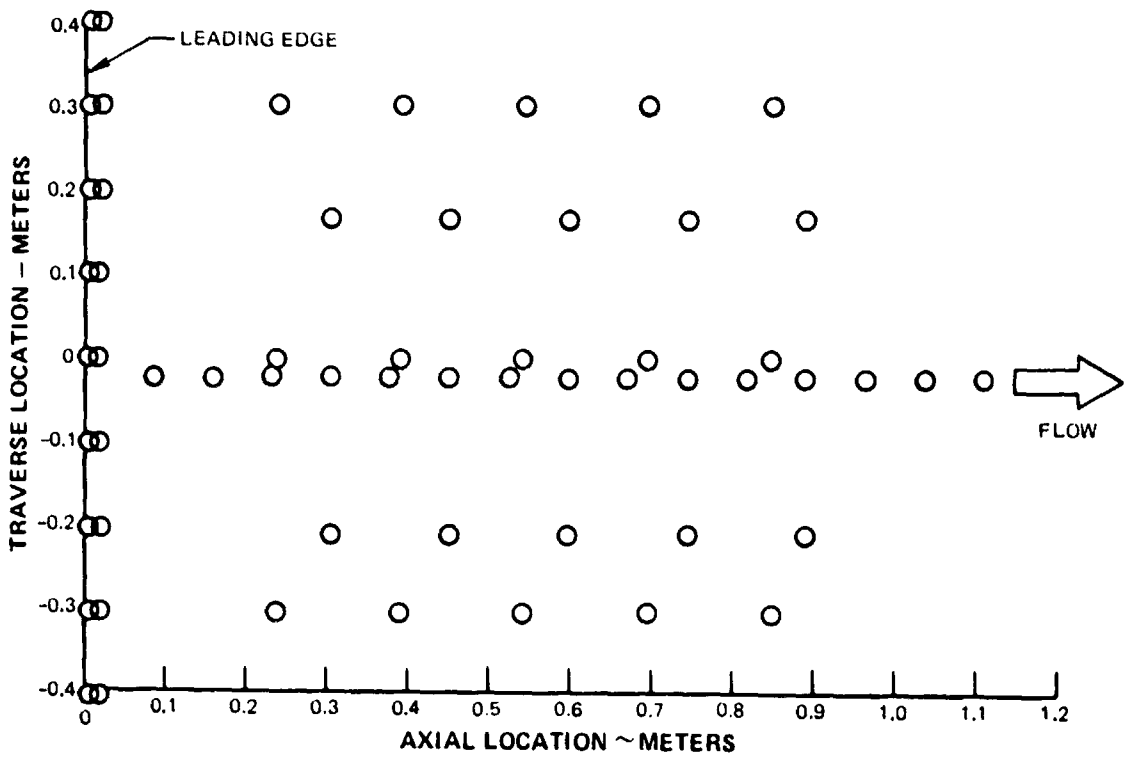

Figure 7 Static Pressure Tap Positions on Test Plate

4.2.2 Transition Identification, Probes, and Circuitry

Flush-mounted, hot-film sensors were used to identify the regions of laminar, transitional, and turbulent flows. Since transition originates in the region of the boundary layer near the wall, measurement of heat transfer from flush-mounted sensors is ideal for studying this process.

These sensors were constructed on the end of a steel tube. An alumia coating of the end surface was flush and smooth to within 0.013 mm. This type of construction facilitated moving the sensors from one hole in the test plate to another, making the flow visible in different stages of transition. In this way the development of turbulent bursts in the sublayer could be compared at different axial stations using oscilliscope traces of the hot-film output signals. The location and size of the transition region was determined from these signals. Approximately thirty sensors were used.

A ten-channel anemometer bridge was used to simultaneously operate ten of the sensors. An electronic processor was built to analyze the output signal from these sensors. The output of the processor was a steady voltage proportional to the intermittency of the flow. A schematic of the processor is shown in Figure 8.

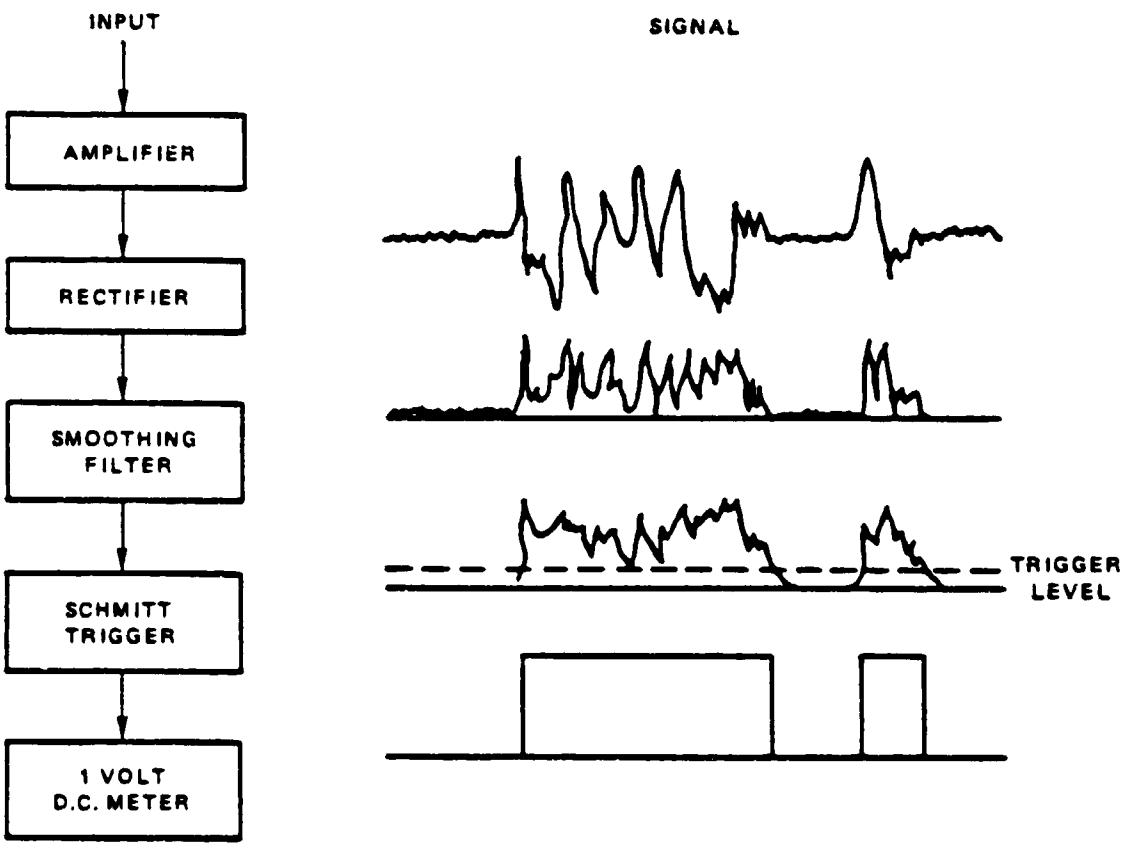

Figure 8 Schematic of Intermittency Meter, Showing Steady Voltage Output Proportional to Intermittency of the Flow

4.2.3 Hot-Film Probes

The reference speed in the wind tunnel was set using pneumatic probes. All other velocities were measured with cylindrical hot-film sensors. Goose-necked, boundary-layer sensors were used to measure the streamwise velocity component and the transverse velocity component parallel to the test wall. The probes (Thermal Systems, Inc., Model 1218G-20 as shown in Figure 9) had a sensing area 0.051mm in diameter and 1mm in length. Similar sensors, (Thermal Systems, Inc., 1243-30 as shown in Figure 10), but of the cross-sensor type, were used to measure the normal velocity component perpendicular to the test wall and the turbulent shearing stress.

Research-quality anemometers, linearizers, signal conditions, and root-mean-square meters were used to obtain a high frequency response. A narrow-band spectral analyzer was used to continuously check for probe vibrations that could contaminate the fluctuating hot-film output signals.

Hot-film sensors were calibrated in a commercially built, low-turbulence, uniform jet. Because the dynamic head of the jet was too low to obtain accurate velocity measurements at the lower end of the calibration range, a novel calibration technique was used in which the velocity was made linearly proportional to the pressure through the use of a choked orifice.

In the calibration system, shown in Figure 11, the choked orifice was adjusted to obtain the desired high velocity in the jet. The reference velocity of the jet, V_{ref}, was determined by measuring the static pressure at the base of the jet with a micromanometer. Decreasing the pressure in the plenum while the orifice size was fixed only changed the density of the flow through the choked orifice and the velocity at the exit of the jet. The new velocity in the jet was then proportional to the reference velocity times the pressure ratio.

This procedure was used for a velocity range of approximately five. The upper limit was determined by the pressure of the air supply; the lower limit, by the minimum pressure that maintained choked flow in the orifice.

After the bridge voltages were measured over the necessary range of velocities, a fourth-order polynomial was fitted to the data by means of a least-mean-square fit. The zero velocity voltage was obtained from the linear extrapolation of E^2 versus U for the two lowest velocity points. After evaluating the coefficients and adjusting them on the linearizer, the calibration was tested in the jet. This testing of the calibrated sensor was performed both before and after the measurements of the mean velocity and turbulence stress profiles.

A typical set of results is shown in Figure 12, a plot of measured velocity divided by actual velocity as a function of actual velocity. The range of velocities covered the entire test spectrum from the lowest velocity measurement near the test section wall to the highest velocity in the free stream. The same procedure was used for a single-element sensor and the cross-wire sensors.

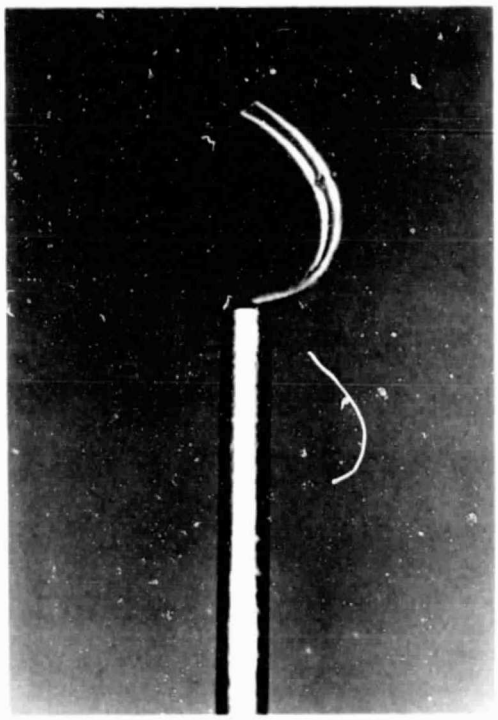

Figure 9 Boundary Layer Probe Single Film to Measure Streamwise mean Velocity and Streamwise and Transverse Componet of Turbulence Intensity

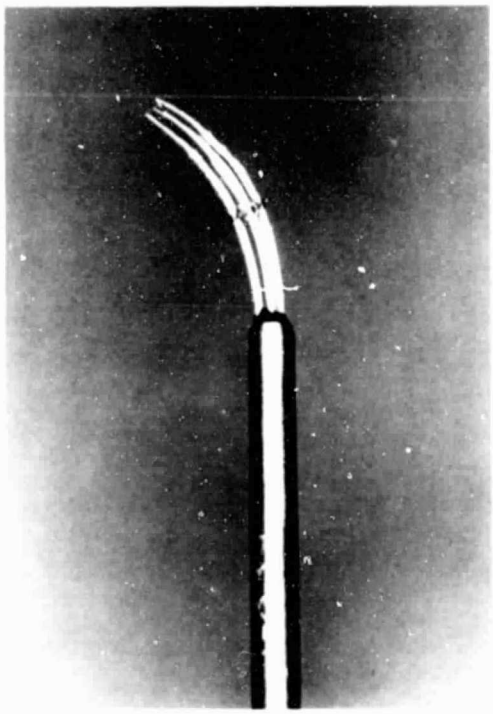

Figure 10 Boundary Layer Probe (cross wire type) to measure normal components of Turbulence Intrensity and Reynolds Sheer Stress

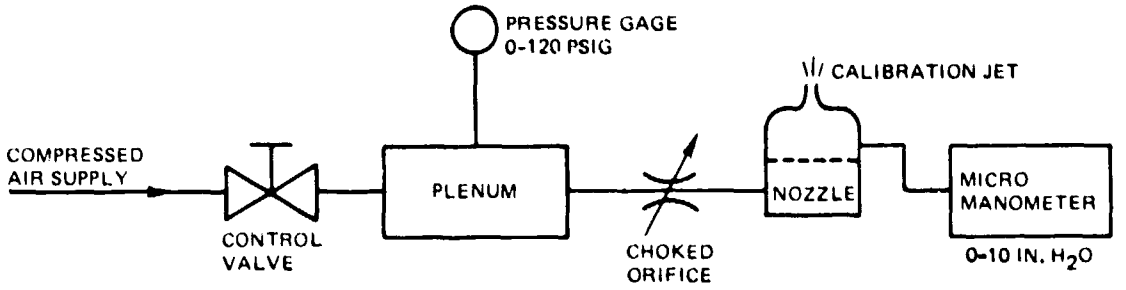

Figure 11 Hot-Film Sensor Calibration System

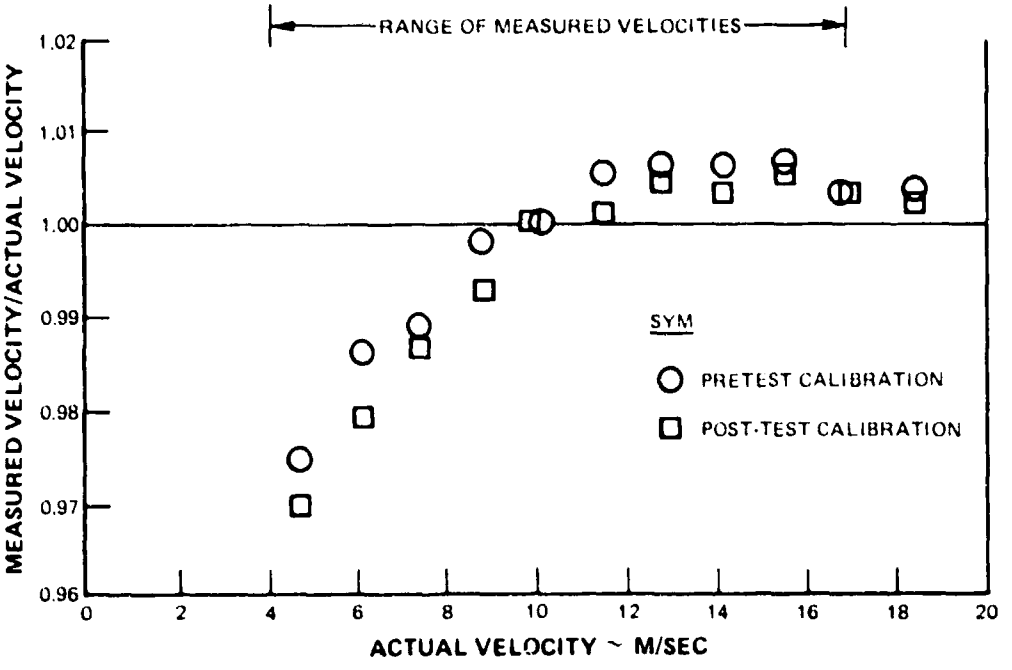

Figure 12 Ratio of Measured-to-Actual Velocities as a Function of Actual Velocity Showing Typical Pretest-Post-Test Calibration Results

4.2.4 Signal Processing and Data Acquisition Equipment

4.2.4.1 Signal Processing

The single-element, hot-film sensor was used to measure the mean velocity and streamwise and transverse components of turbulence intensity. A schematic of the instrumentation is shown Figure 13. Aligning the sensor perpendicular and at $\pm$ 45^0 to the flow resulted in the measurements of

$E = U$ perpendicular to the flow

$e_1 = u$

$e_2 = \frac{u}{\sqrt{2}} - \frac{w}{\sqrt{2}}$ +45^0 to the flow

$e_3 = \frac{u}{\sqrt{2}} + \frac{w}{\sqrt{2}}$ -45^0 to the flow

The constant of proportionality between the voltage and the velocity has been deleated for simplicity.

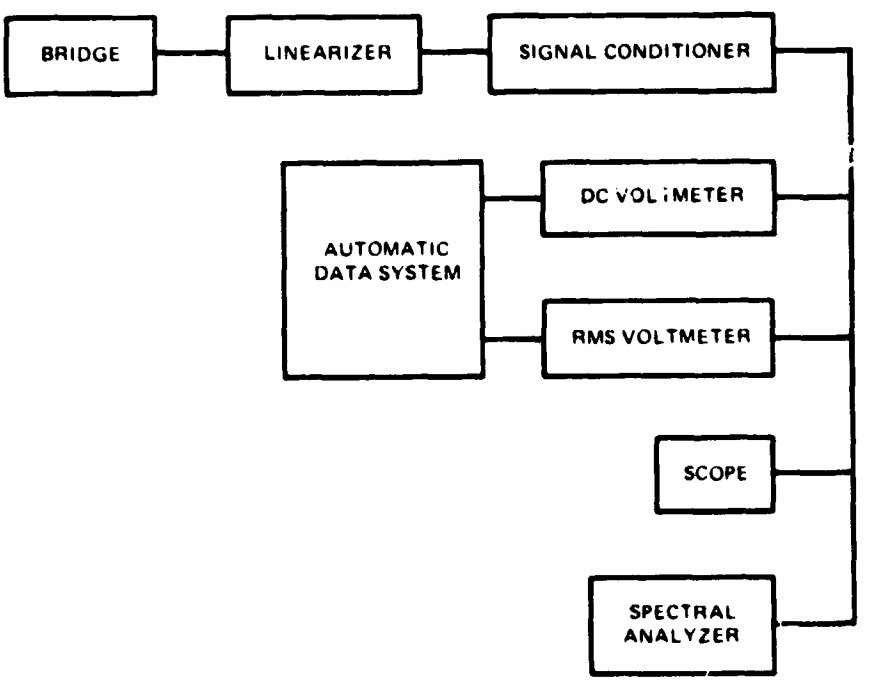

Figure 13 Instrumentation for the Single Channel Hot-Film Sensor

The above measurements can be reduced to:

$$\overline{u^2} = \overline{e_1^{\,2}}$$

$$\overline{w^2} = \overline{e_2^{\,2}} + \overline{e_3^{\,2}} - \overline{e_1^{\,2}}$$

$$U = E$$

The capital letters denote mean velocities and voltages, and the lower case letters denote fluctuating velocities and voltages. The letter U stands for the streamwise velocity, V for the velocity perpendicular to the test wall, and W for the transverse velocity parallel to the test wall.

In the above equations, e_1, e_2, and e_3 were measured during separate traverses. Because the distances from the test wall at which these measurements were made were slightly different, a five-point Lagrangian interpolation was made to determine e_2 and e_3 at the same locations as e_1.

A boundary-layer type cross-sensor probe was used to measure the component of turbulence intensity normal to the wall and the Reynolds shearing stress (-uv). A two-channel anemometer and a sum-and-difference circuit were used for these measurements. A schematic of the instrumentation is shown in Figure 14.

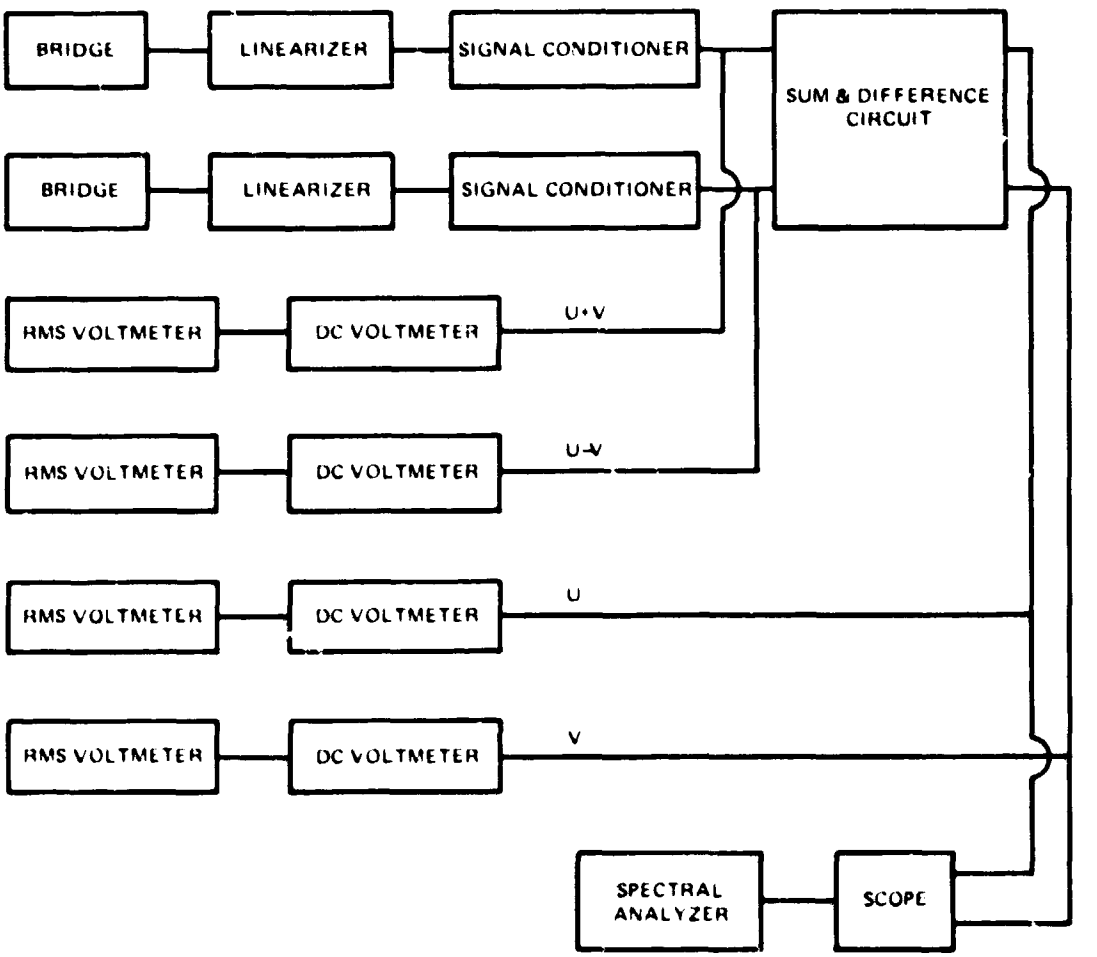

Figure 14 Instrumentation for the Two Channel Hot-Film Sensor

The individual signals from these bridges were

$$e_4 = \frac{u}{\sqrt{2}} + \frac{v}{\sqrt{2}}$$

$$e_5 = \frac{u}{\sqrt{2}} - \frac{v}{\sqrt{2}}$$

The sum and difference of the mean square of the above two equations results in

$$\overline{u^2} + \overline{v^2} = \overline{e_4^{\,2}} + \overline{e_5^{\,2}}$$

$$-2\overline{uv} = (\overline{e_5^{\,2}} - \overline{e_4^{\,2}})$$

The mean square of the sum and difference of the above equations results in

$$\overline{2u^2} = \overline{(e_4 + e_5)^2}$$

$$\overline{2v^2} = \overline{(e_4 - e_5)^2}$$

This permitted simultaneous measurements of $\overline{u^2}$, $\overline{v^2}$, and $\overline{uv}$.

4.3 DATA ACQUISITION SYSTEM

The boundary layer wind tunnel was equipped with an automatic system for data acquisition. This system recorded DC analog voltage signals from the pressure transducer, the hot-film anemometer, and traversing mechanism, and it controlled the movement of the traversing mechanism, which positioned the probes during the boundary-layer measurements. The pressure transducer was connected to a forty-eight port valve so that a large number of pressure taps could be rapidly measured in sequence. The data system was programmed to scan the forty-eight pressure taps, which included total pressure and wall static pressures, before and after each velocity profile. Thus, any drift in the wind-tunnel flow velocity would be noticed. All pressure measurements were obtained with this method. Static pressure taps were manually connected to the switch when more than forty-eight measurements were required.

Two additional input channels, which were available for data from the hot-film anemometer, automatically recorded the mean and fluctuating voltages during the measurements of u^2 and w^2. The root mean square of the fluctuating velocity was converted to a DC analog signal which could be recorded by the data system. The number of required inputs for measuring $-\overline{uv}$ exceeded that of the data system, requiring manual recording.

These data were stored on magnetic disk by the data acquisition system and later reduced and analyzed using the central computing facility.

SECTION 5.0

TEST PROGRAM

5.1 TEST PLAN AND PROCEDURES

The test portion of this investigation was directed towards determining the effect of the shape of the free-stream velocity distribution on the development of two-dimensional boundary layers. Each test section was installed in the boundary-layer tunnel, and the pressure distribution on the test plate at a prescribed exit dynamic head* was compared with the designed pressure distribution. Minor modifications were then made to the contoured surface to provide the desired pressure distribution.

Once satisfactory distribution was obtained, flush-mounted hot films were used to identify regions of laminar, transitional, and turbulent flows. After the various flow regimes had been identified, the mean and turbulence velocity profiles were measured at various locations in the streamwise direction.

Mean-velocity profile data were integrated to determine boundary layer parameters that indicated development of loss through the test section for each test condition. The following characteristics of boundary layer were studied at the specified number of streamwise locations for two specified shapes of free-stream velocity distributions:

a. Mean velocity profile (10 stations)

b. Streamwise component of turbulent intensity (10 stations)

c. Normal component of turbulent intensity (5 stations)

d. Transverse component of turbulent intensity (2 stations)

e. Reynolds shear stress profile (5 stations)

f. Boundary layer integral parameter development (momentum thickness, displacement thickness, shape factor and skin friction at 10 stations).

A differential type of boundary-layer solution, consisting of the McDonald-Fish[3] turbulence model, was evaluated with the above data. The boundary layer procedure was then used to estimate behavior of the two airfoil configurations at low and high Reynolds numbers for high turbulence levels, so as to predict the profile loss behaviors at engine cruise and takeoff conditions.

*Dynamic Head = $\rho U_e^2/2$
where ρ = density and U_e is the exit velocity:
for squared-off configuration U_e = 13.2 m/sec (43.4 ft/sec),
for aft-loaded configuration U_e = 12.6 m/sec (41.4 ft/sec).
Total Temperature = 65°F
Total Pressure = 1 Bar (atmosphere)

5.2 EXPERIMENTAL TECHNIQUES

5.2.1 Flow Visualization

The boundary-layer flow was made visible during the test with the squared-off pressure distribution by injecting ink through the wall pressure taps in the diffusing part of the test section. The ink streaked beyond the end of the diffusing section without any indication of flow separation or converging flow. Traces of these ink streaks are shown in Figure 15. The parallel lines show that there was little three dimensionality of the flow at the wall.

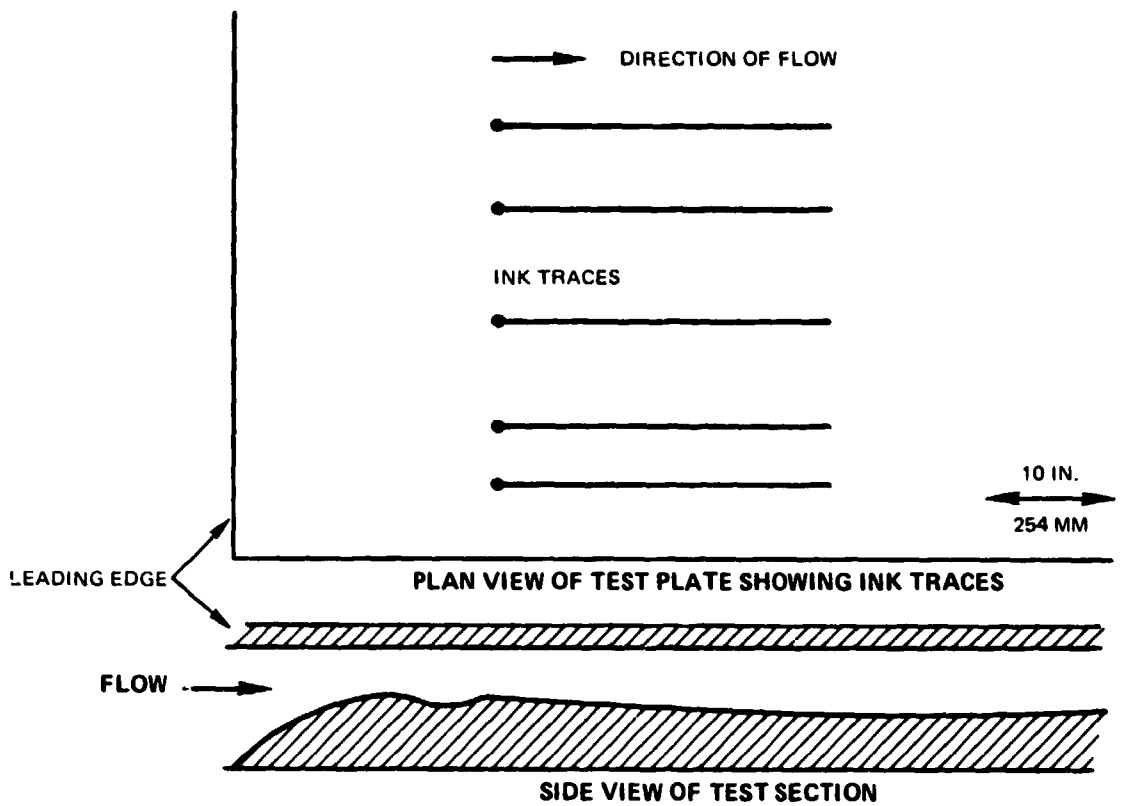

Figure 15 Ink Trace Flow Visualization During Fore-Loaded Test

5.2.2 Wall Static Pressure

The distribution of static pressure on the test plate was measured at the streamwise and cross-stream locations shown in Figure 7. Variations in static pressure in the cross-stream direction were found to be within ± 1 percent of the mean value at all streamwise locations. The pressure coefficients for both the squared-off and aft-loaded sections are plotted along the length of the section in Figure 16. The theoretical pressure distributions used for simulating the suction surfaces of the two sections are also shown. Comparisons between the data and the theoretical distribution are good, indicating that proper simulation of the suction surfaces had been obtained.

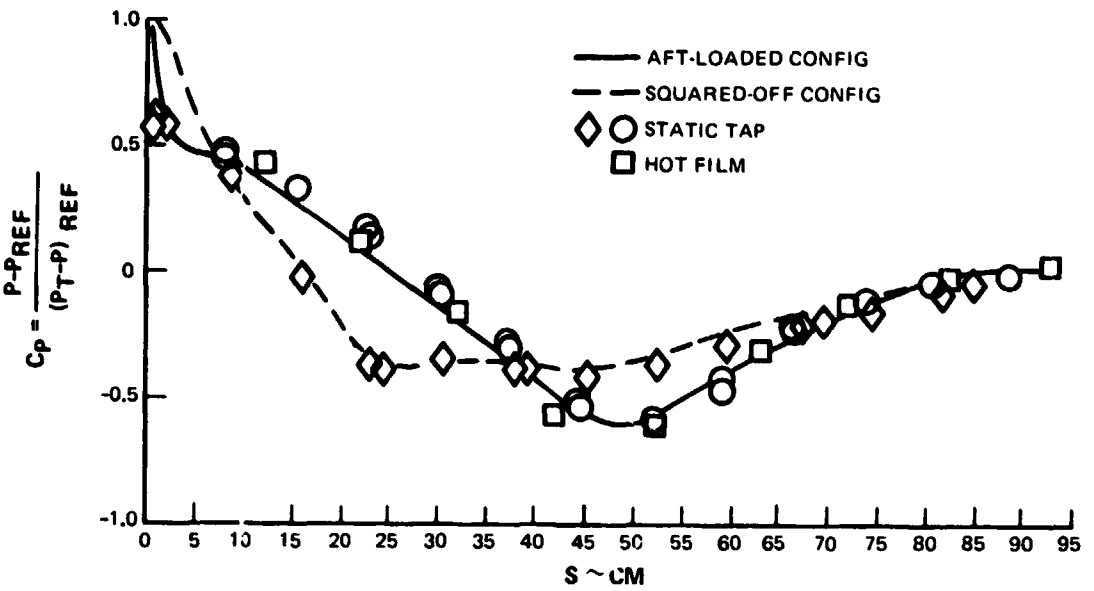

Figure 16 Wall Static Pressure Coefficient as a Function of Test Section Length

5.2.3 Transition

Following Owen[14] and Sharma[15], the transition regions on the two sets of boundary layers were identified using flush-mounted hot-film probes. Figures 17 and 18 show photographs of oscilloscope traces using output signals from these probes for the squared-off test condition, each trace corresponding to a sensor at a streamwise location. The appearance of laminar instability, generation of turbulent fluctuations, and subsequent growth to fully turbulent flow can be clearly identified in Figure 17 for the squared-off test condition. Figure 18 shows the output signal from the intermittency factor circuit where the four stages of the signal processing procedure are shown. The first trace in Figure 18 is the output signal from the hot-film probe, the second is the filtered signal, the third is the rectified signal, and the fourth is the output from the Schmidt trigger obtained by firing the Schmidt trigger when the rectified signal became larger than a specified level.

The root mean square of the fourth signal was taken on the measurement of intermittency factor. The intermittency factor was zero for laminar flows and one for turbulent flows. By definition, the intermittency factor is the fraction of time during which the boundary layer is turbulent.

Dhawan and Narasimha[8] correlated the distribution of intermittency factor as a function of dimensionless distance on the basis of the turbulent spot formation theory of Emmons[9]. The correlation may be written as

$$\gamma = 1 - e^{Z} \qquad (5\text{-}1)$$

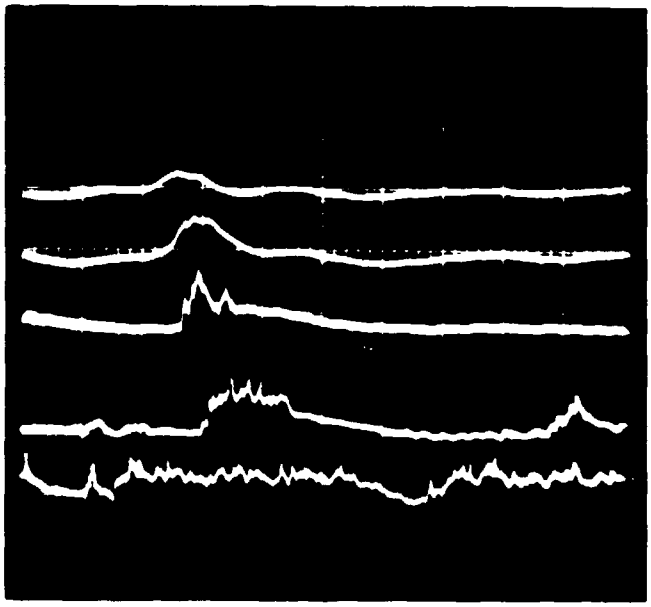

STREAMWISE LOCATION S (METER)	INTERMITTENCY FACTOR (γ)
0.4668	0.0
0.4922	0.04
0.5429	0.10
0.5938	0.45
0.6054	0.92

Figure 17 Oscilloscope Traces From Flush-Mounted Hot-Film Probes for Squared-Off Test Section Showing Growth to Fully Turbulent Flow

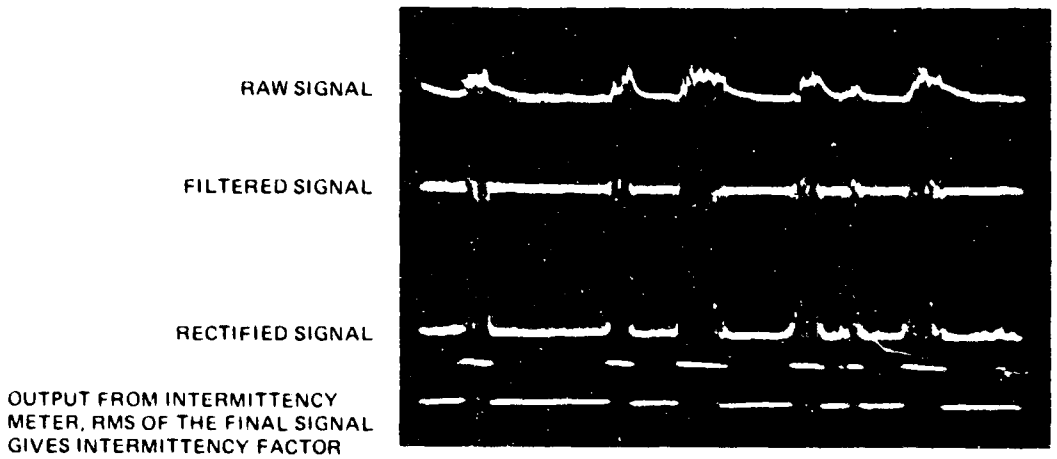

Figure 18 Signal Processing of Hot-Film Probe, Showing Output Signal From Intermittency Meter

where

$$z = -0.412 \left[\frac{s - s_T}{\lambda} \right]^2 \qquad (5\text{-}1a)$$

s = location streamwise distance

s_T = origin of transition location

λ = measure of transition length = $s_{\gamma = .75} - s_{\gamma = .25}$ (see, for example, Figure 19)

From the data of Dhawan and Narasimha[8], Dunham[16] observed that λ could be estimated as

$$\lambda = (s_t - s_T)/3.36 \qquad (5\text{-}2)$$

where s_t is the location where transition region ends and fully turbulent flow begins.

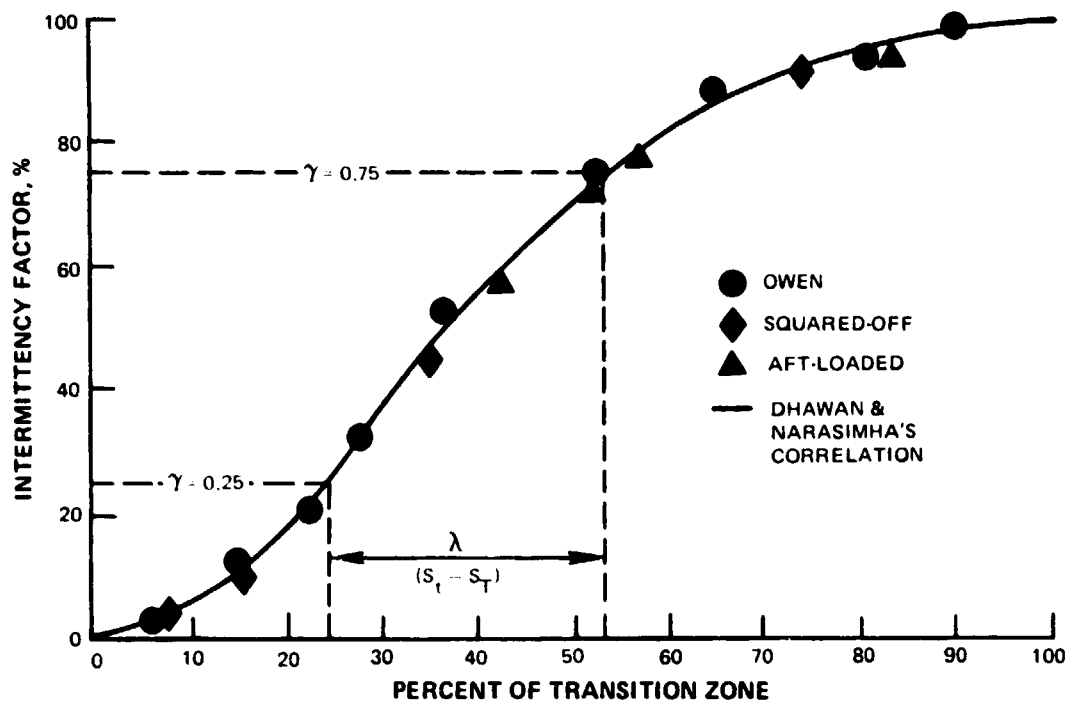

Figure 19 Distribution of Wall Intermittency Data, Showing Data Both From the Program Tests and Other Investigations

Using equations 5-1 and 5-2, the intermittency factor can be written

$$\gamma = 1 - e^{Z_2} \tag{5-3}$$

where $$Z_2 = -4.65 \left[\frac{s - s_T}{s_t - s_T}\right]^2 \tag{5-3a}$$

Dhawan and Narasimha claimed that the distribution of intermittency factor given by equation 5-1 is of a universal nature. Their data base, however, was limited to flows with a zero pressure gradient. In the present investigation, the transition region was located in the diffusing part of the boundary layer; the universal nature of the intermittency factor distribution in diffusing flows is discussed in Section 6.1.

5.2.4 Mean Velocity and Streamwise and Transverse Components of Turbulence Intensity Profiles Velocity

The mean velocity and streamwise components of turbulence intensity profiles were measured with a boundary-layer, hot-film gooseneck probe at ten locations for each of the two test configurations. Nine locations were chosen on the duct centerline for the purpose of obtaining the required velocity and streamwise components of turbulent intensity profiles for the boundary layer. Two profiles were measured at the end of each test section. Five of the profiles were obtained in the diffusing part of the test sections in order to ensure comprehensive coverage of the turbulent boundary layer regime and to improve the accuracy of the profile loss estimate.

5.2.5 Turbulence Intensity and Reynolds Shear Stress Data

Measurements of Reynolds shear stress ($-\overline{uv}$) and the normal component of turbulent intensity were obtained at five streamwise locations for each of the two test configurations. Measurements of the transverse component of turbulent intensity through the boundary layer were obtained for the two test configurations at two streamwise locations: one in the transitional region, the other in the fully turbulent region.

SECTION 6.0

RESULTS

The boundary layers for both test configurations were laminar near the leading edge of the test plate and became fully turbulent after passing through the transitional regime. A detailed discussion of the measured data and the theoretically predicted values is given in this section for each boundary layer regime. The theoretical predictions were obtained from the STAN-5 version of the Patankar-Spalding[17] boundary layer calculation method, using the turbulence model of McDonald-Fish to facilitate the boundary layer predictions through the transition regimes.

6.1 INTERMITTENCY FACTOR DATA

Measurements of intermittency factor disturbiton in the transitional region of the two test boundary layers were obtained from the flush-mounted hot-film probes and the intermittency meter described previously. These data are plotted in Figure 19 along with the flat-plate data of Owen[14] and the empirical correlation of Dhawan and Narasimha[8], which was developed on the basis of data from transitional boundary layers developing under the influence of a zero free-stream pressure gradient. As shown, the test data are in good agreement with the data of Owen and the correlation of Dhawan and Narasimha. Transition regions at the present test conditions were found to be located in the adverse pressure gradient region, as shown in Figure 20. The good agreement of test data with the Dhawan and Narasimha correlation indicates that the distribution of intermittency factor in transitional flows was independent of the free-stream pressure gradient.

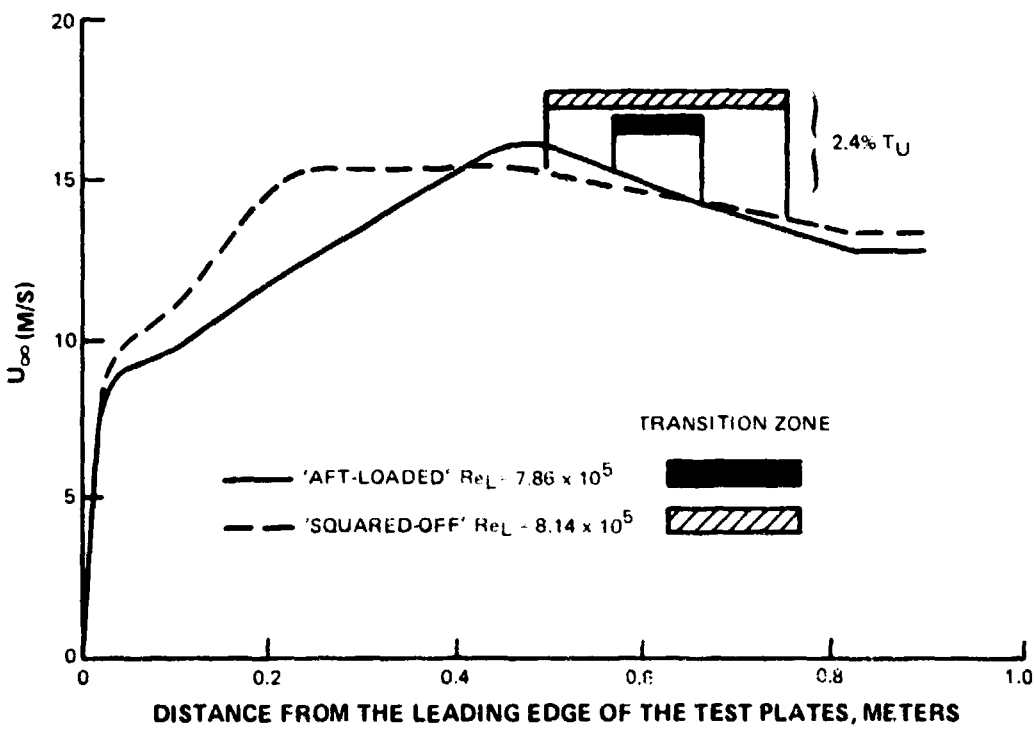

Figure 20 Free-Stream Velocity Distribution and Transition Zones for the Aft-Loaded and Squared-Off Configurations

6.2 MEAN VELOCITY PROFILE

Ten mean velocity profiles were measured for each test geometry. Nine of the combined twenty velocity profiles obtained from both test sections were located in the laminar flow region, four were in the transitional flow region, and the remaining seven were in the fully turbulent flow region. A comparison of the mean velocity profile data in the transitional and turbulent boundary layer regimes with well established semiempirical formulations is discussed in the following paragraphs.

Historically, turbulent velocity profile data are presented in terms of a semilog plot of dimensionless velocity (U^+) vs dimensionless distance from the wall (y^+). Ludwieg and Tillmann[18] showed that all turbulent boundary layer data have a universal region where the following is valid

$$U^+ = \frac{1}{k} \ln y^+ + B \qquad (6\text{-}1)$$

This equation is often referred to as the "law-of-the-wall". The fully turbulent boundary-layer mean-velocity profile data from the two configurations are plotted in Figure 21 using the dimensionless parameters of equation 6-1. There are large regions where the "law-of-the-wall" is valid.

Constants k and B were found to be 0.41 and 5.0, respectively, which is consistent with constants obtained by Coles[11] from the data base presented at the Stanford Conference.

Unlike turbulent boundary layers, no set of comprehensive formulation for the mean-velocity profiles exist for transitional boundary layers. As a result the transitional boundary layer data in Figure 22 had to be plotted in the same coordinate system as used for the turbulent boundary layer data in Figure 21. Figure 22 also shows the data for the wall intermittency factor associated with each profile and velocity profiles expected in the viscous sublayer and in the fully turbulent flows. The figure shows that as the intermittency factor increased, the velocity profiles changed from a viscous sublayer shape to a fully turbulent shape. The velocity profile for the boundary layer, where the intermittency factor was 0.986, exhibited a profile shape similar to the velocity profiles in Figure 21.

6.2.1 Comparison of Test Data With Theoretical Predictions

Integral parameters defined by the momentum loss thickness Reynolds number (Re_θ), the shape factor (H), and the skin-friction (C_f) were calculated from the mean-velocity profile data. Test data were compared with theoretical predictions for the two test boundary layers. Free-stream velocity distributions, shown in Figure 20, and measured inlet turbulence level (Tu = 2.4%) were input parameters for calculating the boundary layer with STAN-5. Theoretical calculations were started with the velocity profile measured at the station nearest the leading edge of the test plate.

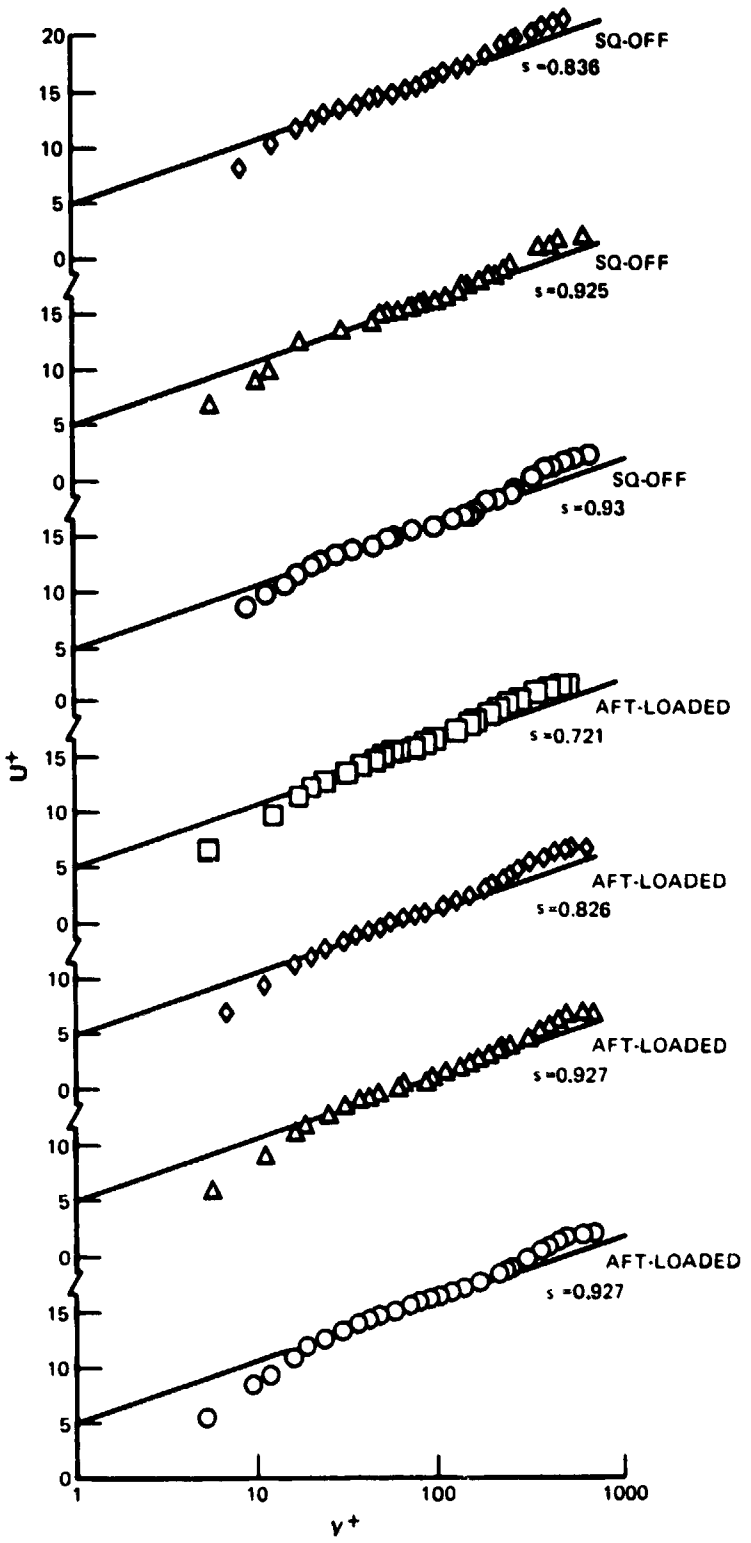

Figure 21 Turbulent Boundary Layer Velocity Profiles for Aft-Loaded and Squared-Off Configurations, Using Law-of-the-Wall Parameters

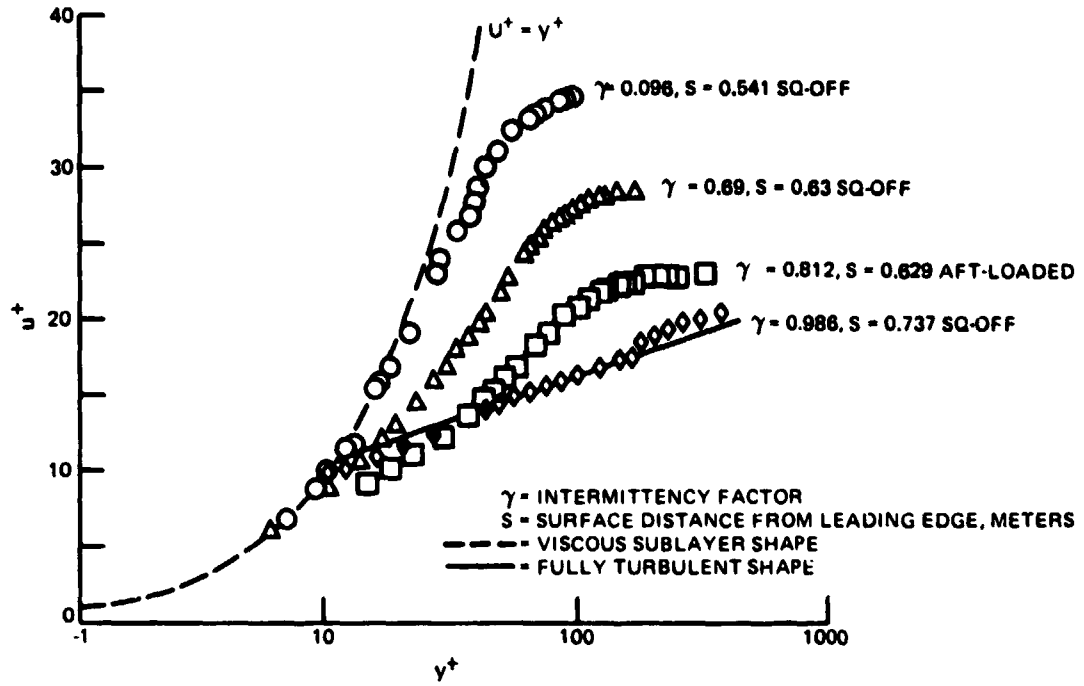

Figure 22 Transitional Boundary Layer Velocity Profiles for Aft-Loaded and Squared-Off Configurations, Using Law-of-the-Wall Parameters

6.2.1.1 Squared-Off Configuration

Experimental data (see Table I) for the integral parameters from the squared-off configuration are plotted in Figure 23 along with predicted values. In general, the predictions were in good agreement with test data.

Detailed mean-velocity-profile data are compared with predictions in Figure 24. The predictions were in good agreement with laminar and turbulent velocity profiles, but in poor agreement with the transitional velocity profile data.

6.2.1.2 Aft-Loaded Configuration

A comparison of experimental and theoretical integral parameters are shown in Figure 25 for the aft-loaded test. Table II gives integral parameters for the aft-loaded test. Predictions and test data were in good agreement for the accelerating part of the flow, but showed flow separation in the diffusing part. The calculations were repeated, and the boundary layer was artifically made transitional at a distance of two boundary layer thicknesses upstream of the expected separation point in order to obtain theoretical predictions*. It should also be pointed out that the calculated separation location was slightly upstream of the transition region identified with the hot-film probes.

*Flush-mounted hot-films in the region close to the predicted separation location gave no indication of the unsteadiness usually associated with separation.

TABLE I

SQUARED-OFF TEST

S (M)	U_∞ (M/S)	$R_{e\theta}$	H	C_f
0.13	11.806	132.7	2.3	.0053
0.302	14.372	221.5	2.52	.00255
0.348	14.615	241.0	2.47	.00185
0.429	15.133	265.9	2.4	.0015
0.541	14.274	358.9	2.25	.001
0.63	13.743	447.7	1.98	.0025
0.737	13.24	681.1	1.48	.005
0.836	12.675	893.3	1.44	.0046
0.925	13.353	1296.4	1.43	.00425
0.93	12.329	1198.4	1.43	.00425

TABLE II

AFT-LOADED TEST

S (M)	U_∞ (M/S)	$R_{e\theta}$	H	C_f
0.121	9.656	126.6	2.28	.00565
0.221	11.945	171.1	2.24	.0037
0.319	13.774	214.0	2.21	.0031
0.419	16.026	244.8	2.19	.0021
0.523	16.206	280.8	2.38	.00185
0.629	14.624	527.5	1.88	.0038
0.721	13.554	880.8	1.44	.00465
0.826	12.981	1130.7	1.43	.0043
0.927	12.582	1291.7	1.42	.00415
0.927	12.512	1310.1	1.42	.00415

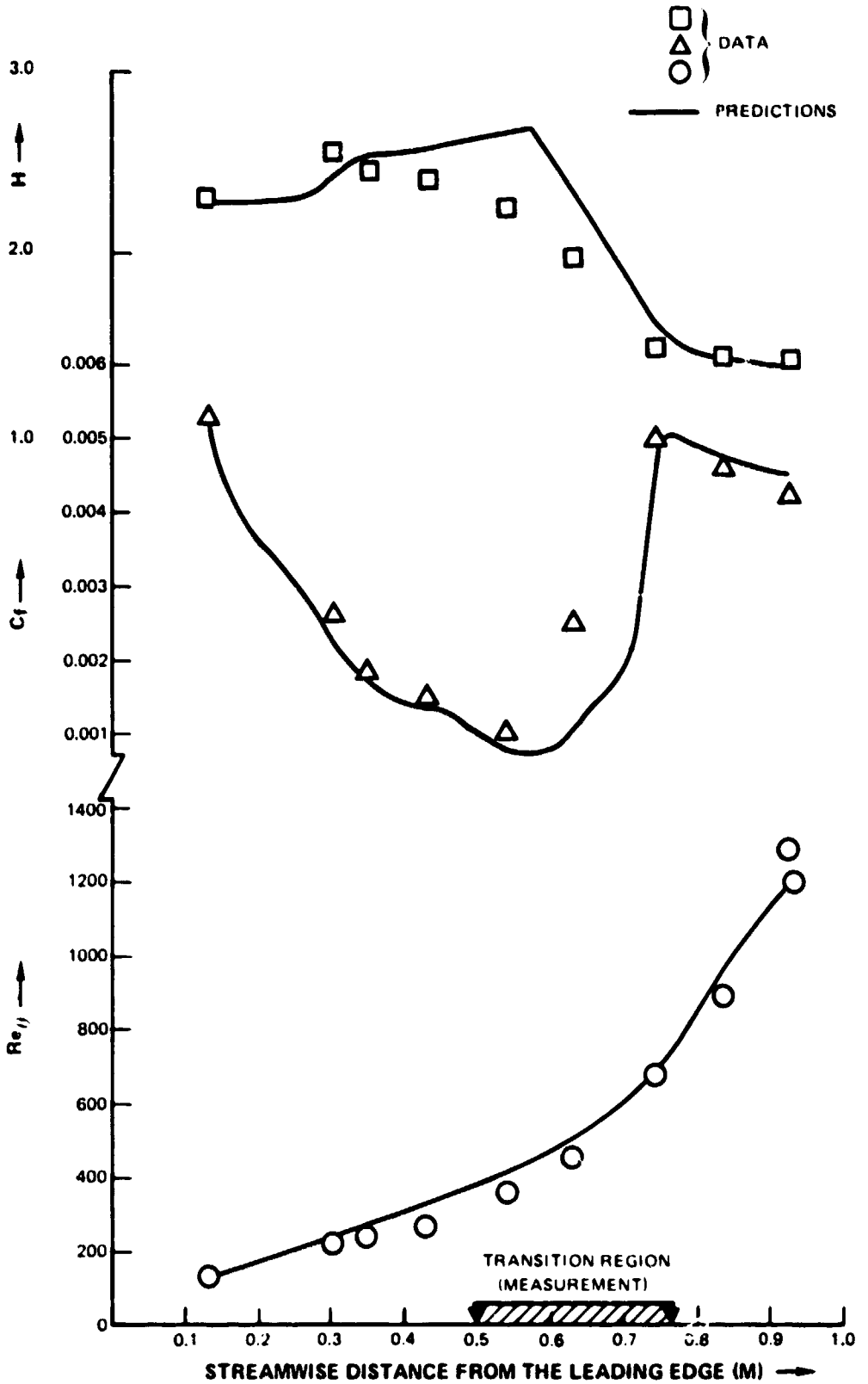

Figure 23 Comparison of Measured Integral Parameters for Squared-Off Configuration With Predictions Obtained With McDonald-Fish Turbulence Model

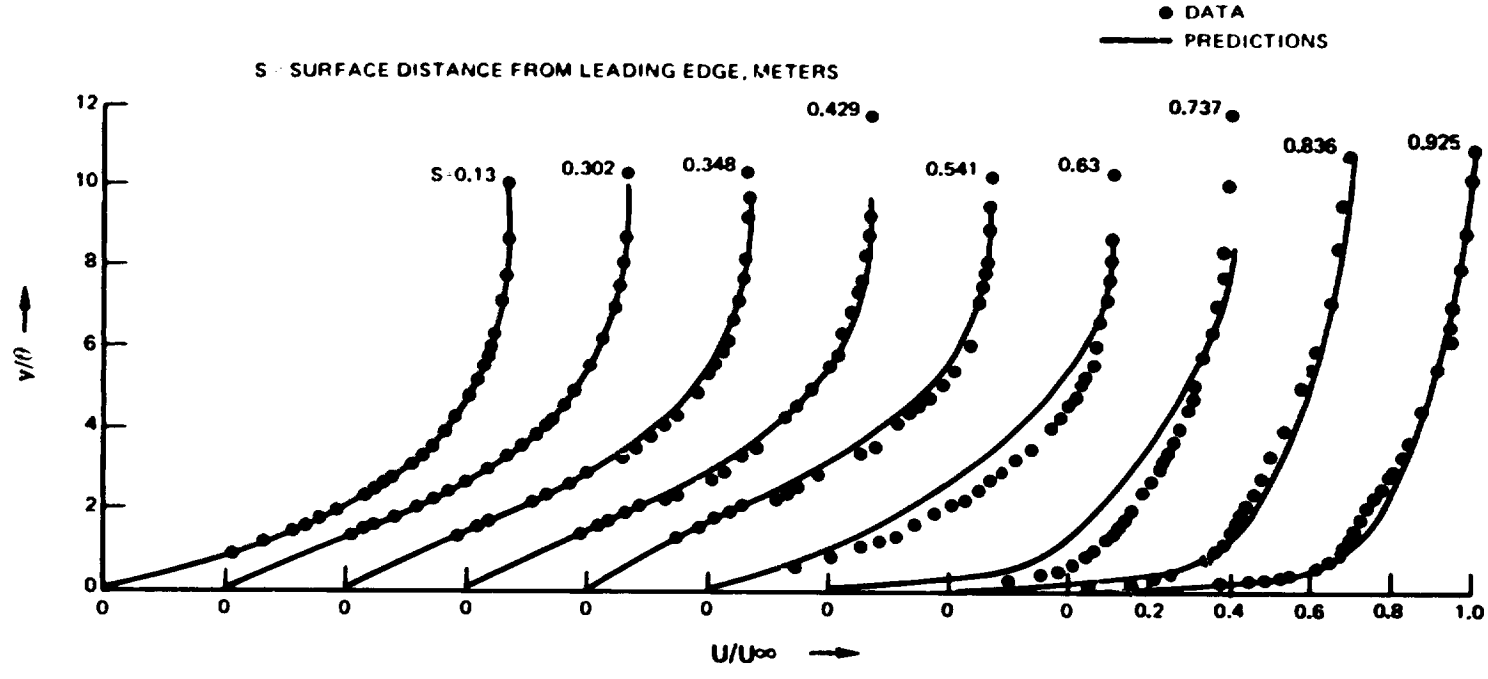

Figure 24 Comparison of Measured Mean Velocity Profile Data for Squared-Off Configuration With Predictions Obtained with McDonald-Fish Turbulence Model

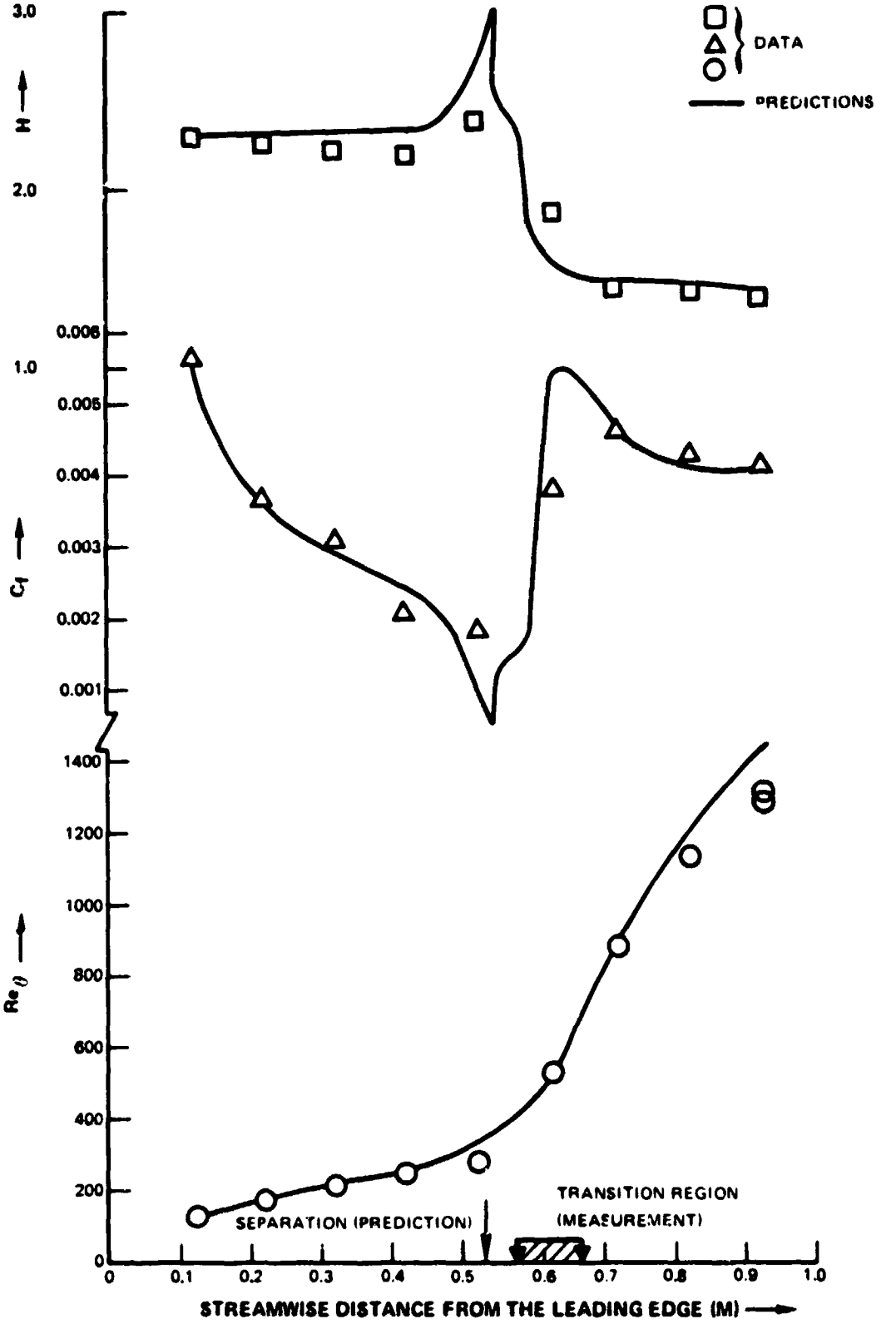

Figure 25 Comparison of Measured Integral Parameters for Aft-Loaded Configuration With Predictions Obtained With McDonald-Fish Turbulence Model

Figure 26 provides detailed velocity profile data along with predictions. Again, measured and predicted mean-velocity profiles were in good agreement for the laminar and turbulent regions.

Comparisons of theoretical predictions with the experimental data for the two test configurations indicated that the McDonald-Fish turbulence model provided overall good estimates for the mean integral parameters for attached transitional boundary layers.

6.2.2 Comparison of Squared-Off and Aft-Loaded Data and Assessment of Profile Losses

6.2.2.1 Momentum Loss Thickness

Development of momentum deficit thickness for the two test boundary layers is plotted in Figure 27. At the exit plane in the test section, momentum deficit thickness for the aft-loaded test is about 9 percent larger than that for the squared-off test. This result would show that the squared-off airfoil would yield 9 percent lower loss than the suction surface losses for the aft loaded airfoil. Assuming that the pressure surface losses for both of these airfoils were the same and about 20 percent of the squared-off suction surface loss, then the squared-off airfoil would result in about an 8 percent lower profile loss than the aft-loaded airfoil. However, it should be emphasized that this result is correct only at the present test condition: a high Reynolds number and a relatively low turbulence level. Profile loss behavior as a function of Reynolds number and turbulence level is discussed in the following section for these two airfoils.

An interesting observation about the growth rate of momentum deficit thicknesses for the present two test boundary layers can be made from Figure 27. Momentum deficit thickness developmemt for the aft-loaded configuration shows two distinct regions of development: one associated with laminar flows, the other with turbulent flows. There seems to be an abrupt change from laminar to turbulent region with a rather short region for transitional flows. Data for the squared-off test show a gradually varying between the laminar and turbulent flow regimes. This observation points out that while the squared-off airfoil boundary layer transformed from laminar to turbulent flows through a large region of natural transition flow, the laminar boundary layer in the aft-loaded test under went transition in a short distance and became turbulent, generating higher momentum loss thickness in the process. It should be pointed out that flush-mounted hot-film probes in the laminar and transitional regions of the flow field for the aft-loaded configurtion gave no indication of the unsteadiness usually associated with separation.

6.2.2.2 Shape Factor

The distribution of boundary layer shape factor, $H = \delta^*/\theta$, is illustrated in Figure 27b for both boundary layers. The two distributions, remarkably similar in the laminar regime, are characterized by a value of 2.3, decreasing to 1.4 in the turbulent regime.

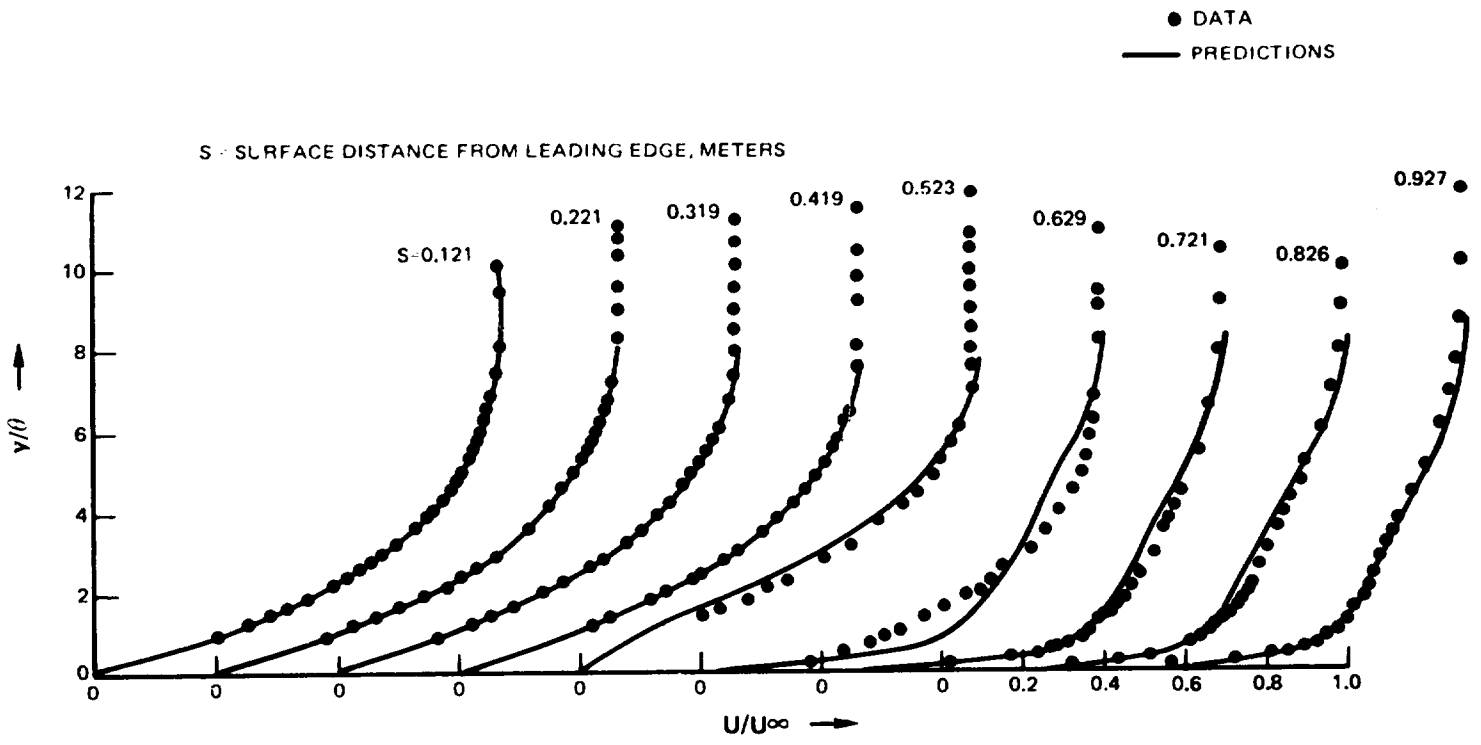

Figure 26 Comparison of Measured Mean Velocity Profile Data for Aft-Loaded Configuration With Predictions Obtained With McDonald-Fish Turbulence Model

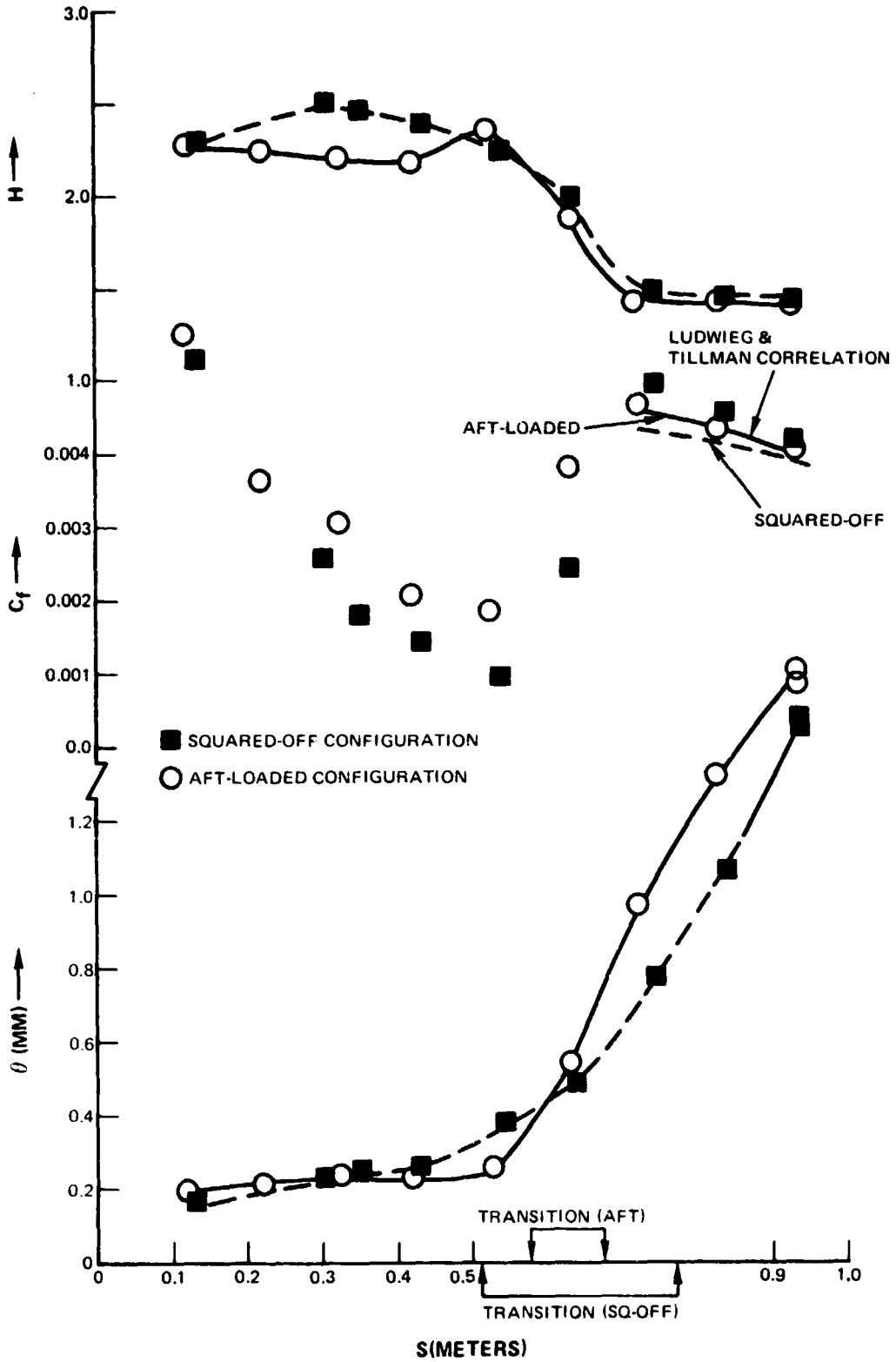

Figure 27 Distribution of Momentum Loss Thickness (Re_θ), Shape Factor (H), and Skin Factor (C_f) for the Aft-Loaded and Squared-Off Configurations

The shape factor associated with the aft-loaded test increased prior to the transition region, lending further evidence that the adverse pressure gradient was the dominating mechanism initiating transition for this test condition.

6.2.2.3 Skin-Friction

Streamwise distribution of skin friction (C_f), inferred from the mean velocity profile data, is plotted in Figure 27c for the two test boundary layers. The values of skin friction deduced from the Ludwieg and Tillman correlation for the turbulent region are also plotted in the figure. The agreement between the correlation and present data is good.

6.3 BOUNDARY LAYER TURBULENCE INTENSITY PROFILES

6.3.1 Turbulent Region

Three components of turbulence intensity were measured through the boundary layer at the exit station for each of the two test configurations. These three components of turbulence intensity were added in order to generate profiles for turbulent kinetic energy profiles for the two test boundary layers.

The turbulence kinetic energy level across the width of each test boundary layer is shown in Figure 28; the distribution of turbulent kinetic energy profile measured by Klebanoff[19] for a flat plate boundary layer is also shown. Data in the above figure show that the turbulent kinetic energy profiles in the fully turbulent region for both test boundary layers have similar shapes and their distributions show fair agreement with the measurements of Klebanoff. Since the measurements of Klebanoff were obatained for an equilibrium turbulent boundary state, the above comparison between the present data and the Klebanoff results shows that the present test boundary layers are reaching an equilibrium state.

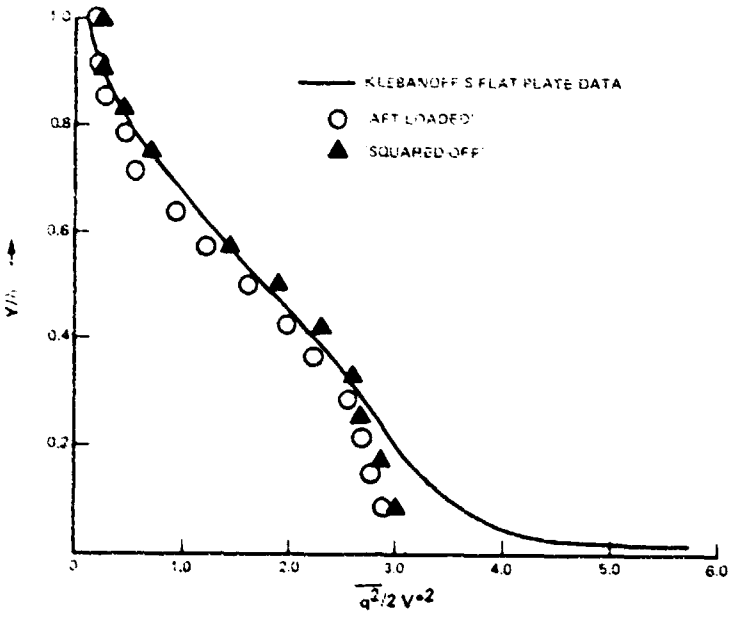

Figure 28 Comparison of Measured Program Total Turbulence Intensity With Flat-Plate Data of Klebanoff

The relative magnitudes of the streamwise ($\overline{u^2}$), normal ($\overline{v^2}$) and transverse ($\overline{w^2}$) components of turbulence intensity are shown in Figure 29 for the two test boundary layers. The data indicate that the streamwise component contained about 50 percent of the total turbulence intensity while the normal component contained about 20 percent, which is consistant with flat-plate data. These values were used in the McDonald-Fish turbulence model.

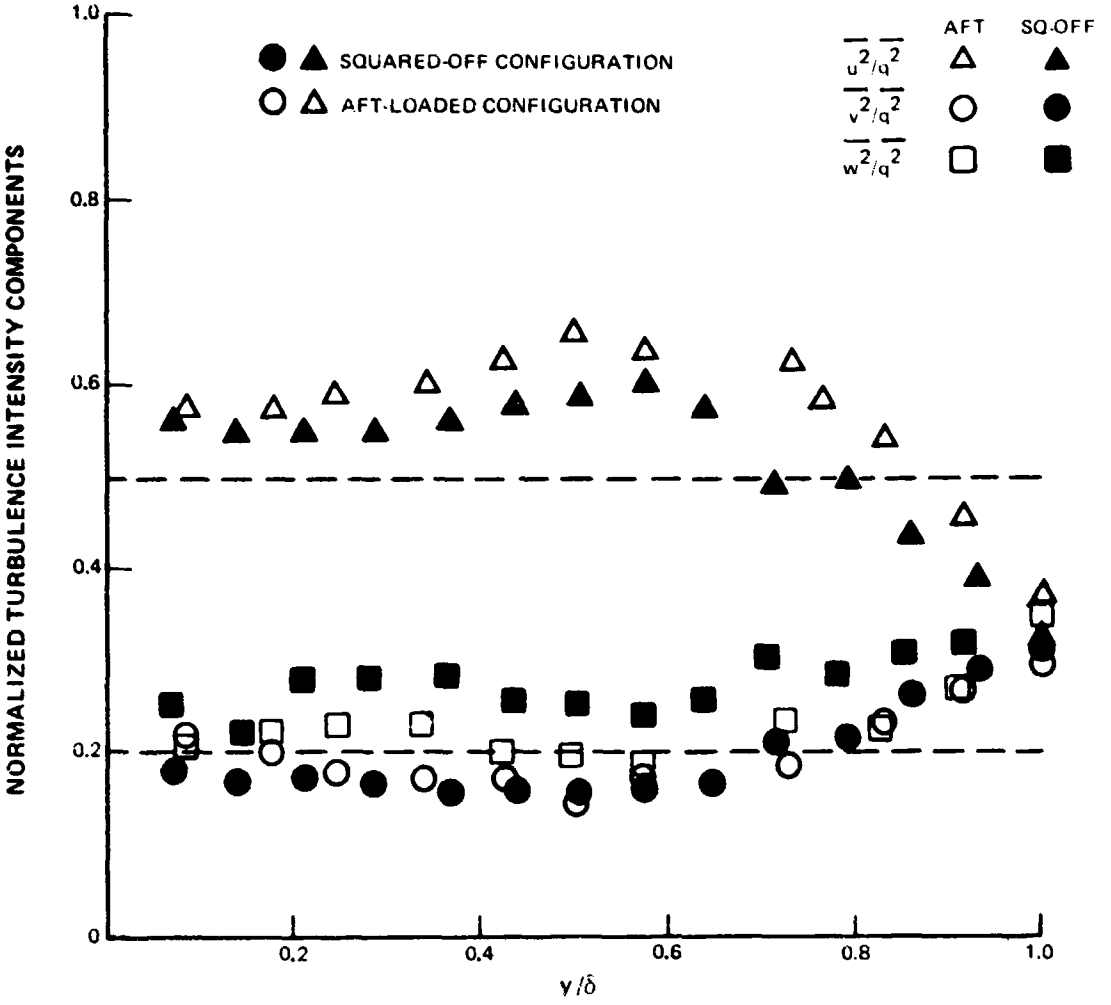

Figure 29 Distribution of Normalized Turbulence Intensity Components in Fully Turbulent Region

6.3.2 Transitional Region

Relative magnitudes of turbulence intensity components for the transitional region of the squared-off test boundary layer are plotted in Figure 30. The test data showed that the streamwise and the normal components contained about 80 and 10 percent of the total turbulence intensity, respectively, which indicated that the turbulence in transitional boundary layers was more nonisotropic than in fully turbulent boundary layers. Lines drawn at 0.5 and 0.2 in this figure indicate the values used by McDonald-Fish in their turbulence model. The present turbulence data indicate that in the transition region the assumptions of McDonald-Fish are not validated by the present data.

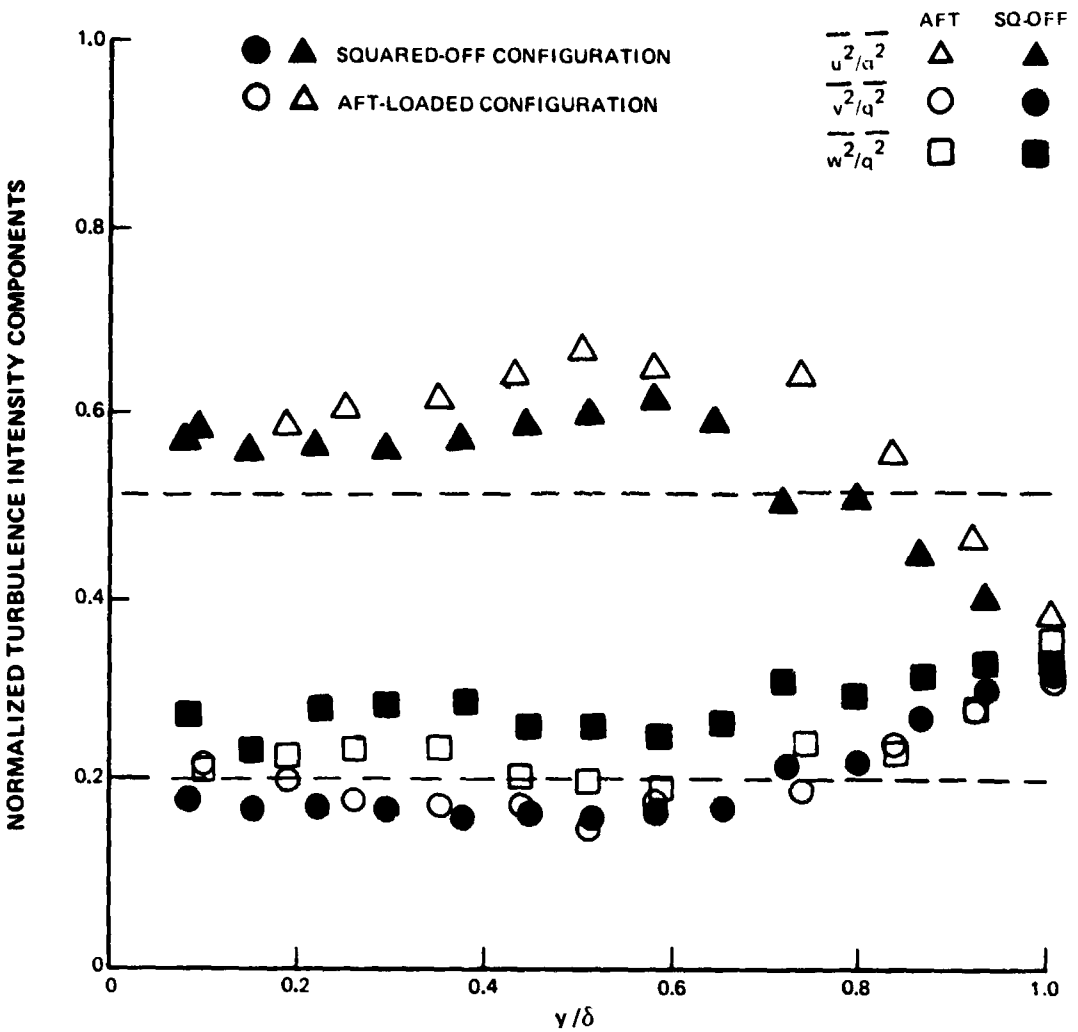

Figure 30 Distribution of Normalized Turbulence Intensity Components in Transitional Region

6.3.3 Laminar Region

Systematic growth of the streamwise component of turbulence intensity was observed in the laminar region of both test boundary layers.

Dimensionless turbulent intensity (u^+) data in the laminar boundary region for both test configurations are presented as functions of y^+ in Figure 31. This figure shows two important features:

1) Turbulence intensity profiles in the laminar region had a maximum value in the neighborhood of $y^+ = 25$.

2) Maximum turbulence intensity (u^+ at $y^+ = 25$) increased in the downstream direction as the onset of transition was approached.

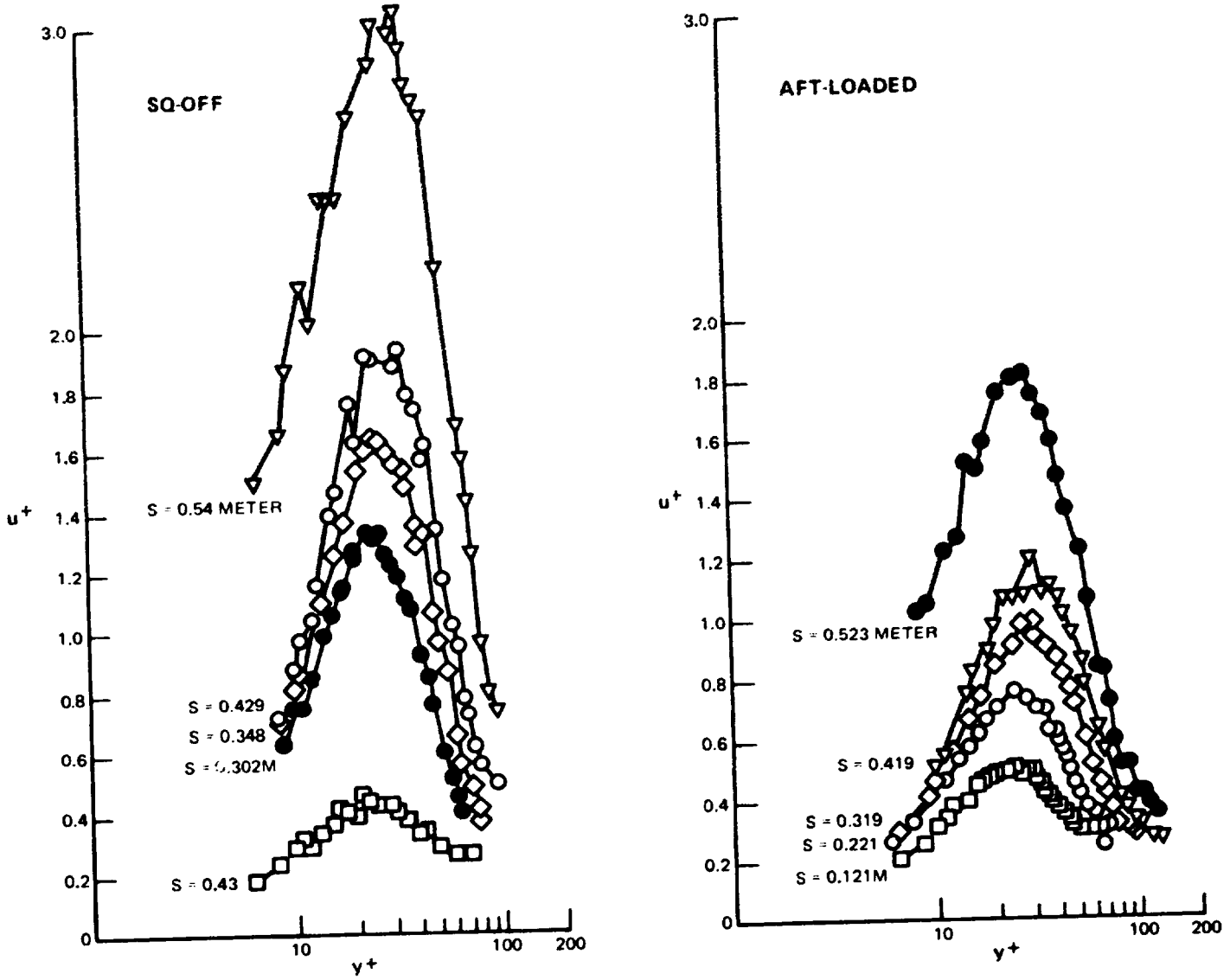

Figure 31 Growth of Turbulence Intensity in Laminar Region of the Squared-Off and Aft-Loaded Configuration Boundary Layers

Similar observations can be duduced from the measurements of Leipmann[8] and Schubauer and Klebanoff[19]. The data from the latter work (plotted in Figure 32) show the same trend as that observed during the Program investigation. Both Leipmann and Schubauer and Klebanoff concluded that these high turbulence intensities were due to the presence of strongly amplified oscillations and that these disturbances do not significantly influence the shape of the mean velocity profiles.

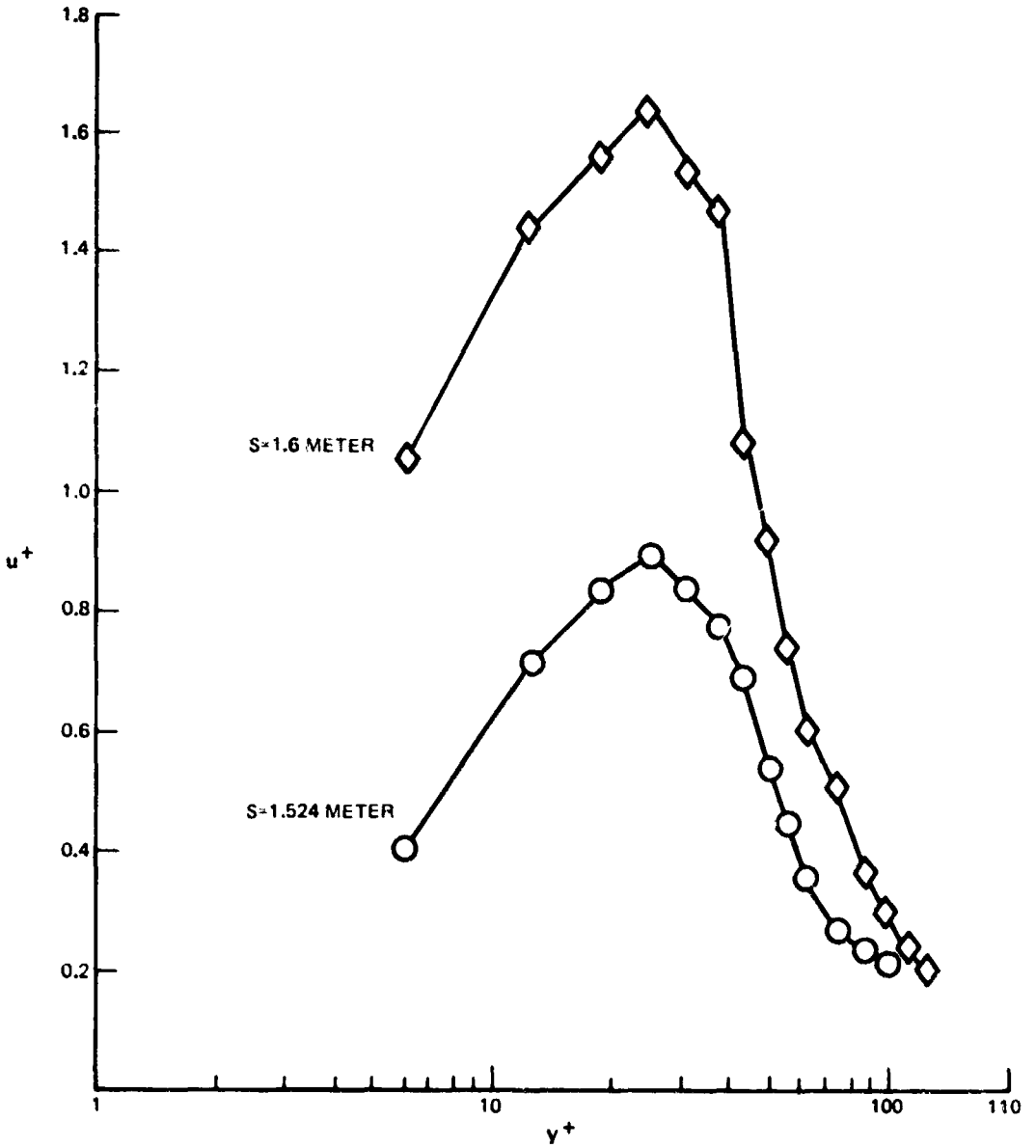

Figure 32 Growth of Turbulence Intensity in the Flat-Plot Laminar Boundary Layer Region as Reported by Schubauer and Klebanoff

The program study and conclusions reported in references 8 and 17 form the basis of a hypothesis for the onset of transition in boundary layer flows. Conceptually, disturbances grow in laminar boundary layers in the streamwise direction until a threshold value is reached where the process of transition is initiated. If the onset of transition is assumed to occur when the intermittency factor reaches about 0.1, then on the basis of the program data, the threshold disturbance value corresponds to $u^+_{max} = 3$.

This hypothesis for the onset of transition may be written as

$$\overline{u^2} = 9 \quad v^{*2} \tag{6-3}$$

Leipmann[8] measured various components of turbulence intensity in laminar boundary layers, and the results indicated that streamwise and normal components of turbulence intensity contain respectively about ninety and four percent of the total turbulence intensity. Leipmann also proposed a hypothesis for the onset of transition according to which flow becomes transitional when the maximum value of Reynolds shear stress in laminar flow equals the wall shear stress. Leipmann's hypothesis for the onset of transition may be written as

$$-\overline{uv} = v^{*2} \tag{6-4}$$

If Leipmann's hypothesis is assumed to be consistent with the hypothesis proposed in this report, then equations (6-3) and (6-4) and the turbulence intensity data of Leipmann may be used to obtain the following relationship between the Reynolds shear stress and total turbulence intensity

$$-\overline{uv} = 0.1\ \overline{q^2} \tag{6-5}$$

It is interesting to note that $-\overline{uv}/\overline{q^2}$ in the laminar boundary layer (equation 6-5) is of the same order as obtained in fully turbulent flows where $-uv/q^2$ is typically 0.12.

Equations (6-3) and (6-4) and Leipmann's data may also be used to obtain typical values of the correlation coefficient between the streamwise and normal components of turbulence intensity. The correlation coefficient (C) may be written in terms of Reynolds shear stress and the two components of turbulence intensity as

$$C = \frac{-\overline{uv}}{\sqrt{\overline{u^2}}\quad\sqrt{\overline{v^2}}} \tag{6-6}$$

Substituting in equation (6-6) v^{*2} for $-\overline{uv}$ from equation (6-4), $\overline{v^2} = 4\ u^2/90$ from Leipmann's data, and $u^2 = 9\ v^{*2}$ from equation (6-3) leads to

$$C = 0.527 \tag{6-7}$$

Since the correlation coefficient (C) is typically of the order of 0.45 in fully turbulent flows, the value in equation (6-7) is in reasonable agreement, implying that the magnitude of correlation coefficient may be independent of the state of the boundary layer.

Several turbulence models (3, 4, 5) implicitly assume that either a variation in correlation coefficient (C) or a variation in $-\overline{uv}/q^2$ is responsible for low magnitudes of Reynolds shear stress in laminar or transitional boundary layers. However, equations (6-5) and (6-7) show that both C and $-\overline{uv}/q^2$ may be independent of the state of the boundary layer. Lower magnitudes of Reynolds shear stress in laminar and transitional boundary layers, as opposed to fully turbulent boundary layers, are possible because of the lower magnitudes of the normal component of turbulence intensity in these flows, impling that the nonisotropic nature of turbulence in laminar and transitional boundary layers may be a dominating mechanism governing the process of boundary-layer transition. None of the available turbulence models recognizes this nonisotropic behavior of turbulence for predicting boundary layer growth.

On the basis of the test data for transitional and turbulent boundary layers and on Leipmann's data for laminar boundary layers, the process of transition may be visualized in the following manner. Disturbances, due to instabilities in the viscous flow, grow in the laminar boundary layer where most of the disturbance energy is contained in the streamwise component. Initially, the normal component of turbulent energy has a low value in the laminar boundary layer, but increases in the downstream direction by gaining energy from the streamwise component. Simultaneously, Reynolds shear stress is generated because of the presence of the normal component. When the maximum value of the Reynolds shear stress is equivalent to the wall shear stress, flow ceases to be laminar and the process of transition is initiated. Both streamwise and normal components of turbulent energy grow in the transitional region with the latter component growing at a faster rate, resulting in an overall increase of the Reynolds shear stress. Transition is terminated when the streamwise and the normal components of turbulence energy and the Reynolds shear stress reach their respective equilibrium magnitudes.

SECTION 7.0

ANALYTICAL ASSESSMENT OF PROFILE LOSSES

The Boundary Layer Program indicated that the McDonald-Fish turbulence model gives reliable predictions for attached transitional boundary layers and is therefore a reasonably good tool for estimating the profile losses for low-pressure turbine airfoils of the Energy Efficient Engine type.

Reynolds numbers in an engine environment vary over a wide range and are usually lower than those achieved in the Boundary Layer Program. Also, turbulence intensities are believed to be higher in an engine environment. Calculations of boundary layer parameters were performed over a wide range of Reynolds numbers and turbulence levels to verify the airfoil design concepts of the low-pressure turbine at high altitude cruise engine operating conditions, using the McDonald-Fish turbulence model.

The fourth-stage mean section of the low-pressure turbine was chosen for comparing the suction-side profile loss of the airfoil design (aft-loaded) of the Energy Efficient Engine with an equivalent airfoil having a squared-off suction-surface design. These airfoils had the same leading and trailing edge geometries, differing in the distribution of thickness in order to provide the desired suction surface velocity distributions.

The McDonald-Fish model was used to calculate boundary-layer development on the suction side of both airfoils over a range of aerodynamic conditions. Inlet turbulence velocity ranged from 1.6 to 10 percent of inlet velocity. Reynolds number and total temperature used in this exercise are shown in Figure 33. These values were taken from the low-pressure turbine design conditions for the Energy Efficient Engine. The same values of static-to-total-pressure distribution were used for each airfoil in representing a stage of the low-pressure turbine for calculation purposes.

7.1 SAMPLE PROFILE LOSS PREDICTIONS

Profile loss can be estimated through a knowledge of the momentum loss thickness at the trailing edge of the airfoil. Experience to date indicates that about 75 to 80 percent of the loss in total momentum is due to the boundary layer on the suction surface of the airfoil.

In order to verify the design concepts of the low-pressure turbine for the Energy Efficient Engine, boundary layer momentum loss thicknesses were calculated at the trailing edge of two equivalent airfoils. If one airfoil was predicted to have a lower momentum thickness at the trailing edge, the corresponding load distribution (static to total pressure distribution on the airfoil surface) was considered to be proper for the Energy Efficient Engine design.

Sample results of boundary layer calculations are presented in Figure 34. These calculations were performed at the design condition for the fourth stage of the low-pressure turbine at cruise altitude. The figure shows development of boundary layer momentum loss thickness Reynolds number, shape factor, and skin friction. These results were obtained at an inlet turbulence level of six percent.

Calculations of momentum loss thickness at the trailing edge of the airfoils revealed that the suction-surface with a squared-off pressure distribution yielded a lower profile loss than with an aft-loaded pressure distribution. This benefit in profile loss was dependent upon the inlet turbulence level and Reynolds number, a result discussed in more detail in Section 7.2.

The calculated distribution of momentum loss thickness Reynolds number on both airfoils was similar to that obtained from the Program tests (Figure 27). On the forward portion of these airfoils, aft-loading imposed an accelerating velocity field on the boundary layer, yielding a low value of momentum loss thickness growth and a low value at the beginning of the diffusion region. For the squared-off airfoil, the region of free-stream velocity acceleration extended over a smaller fraction of the airfoil and was followed by a region with a zero velocity gradient, resulting in a higher growth rate of momentum loss thickness and a higher value of momentum loss thickness at the beginning of the velocity diffusion region.

The effect of the high diffusion factor (ratio of maximum velocity on the airfoil suction surface to the exit velocity) was more severe for the aft-loaded airfoil than for the squared-off airfoil, which resulted in higher momentum loss thickness at the trailing edge of the aft-loaded airfoil than for the squared-off airfoil.

Distributions of shape factor and skin-friction coefficient indicated that boundary layers were laminar over most of both airfoil surfaces. The transitional flow regime was detected near the trailing edge of the airfoil after the point of minimum skin-friction coefficient. Fully turbulent flows were not predicted for either of the airfoils.

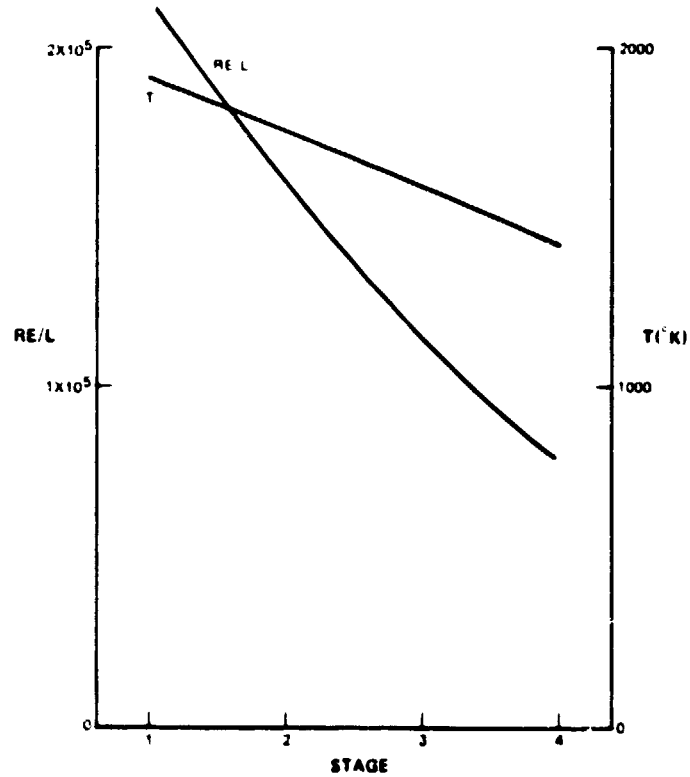

Figure 33 Variation of Reynolds Number and Temperature through the Energy Efficient Engine Low-Pressure Turbine

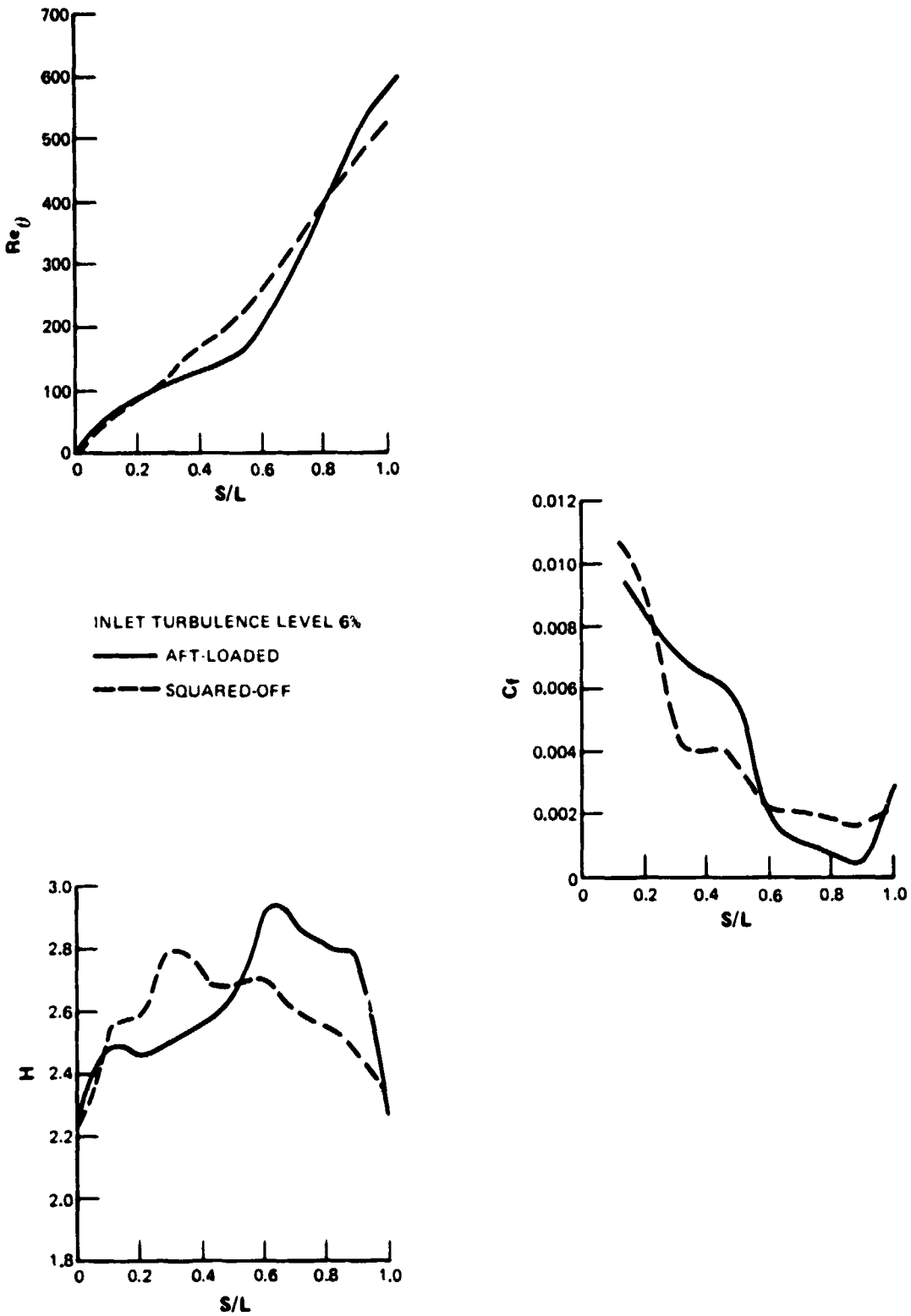

Figure 34 Sample Calculations of Boundary Layer Parameters (Re_θ, H, C_f) Obtained with McDonald-Fish Model

7.2 INFLUENCE OF REYNOLDS NUMBER AND INLET TURBULENCE LEVEL ON PROFILE LOSSES

A range of Reynolds numbers and turbulence levels was investigated to assess the tradeoff in performance between the two airfoils in various flow regimes. The range covered four turbulence levels (1.6, 4, 6, and 10 percent) and Reynolds numbers corresponding to flow conditions relative to the blades of the low-pressure turbine. The influence of Reynolds number on the losses was determined by varying the relative total pressure and total temperature through the low-pressure turbine while maintaining the inlet Mach number constant.

The results of these calculations are shown in Figure 35 for the two pressure distributions. The figure also presents momentum loss thickness as a function of the free-stream turbulence level for constant suction surface Reynolds number.

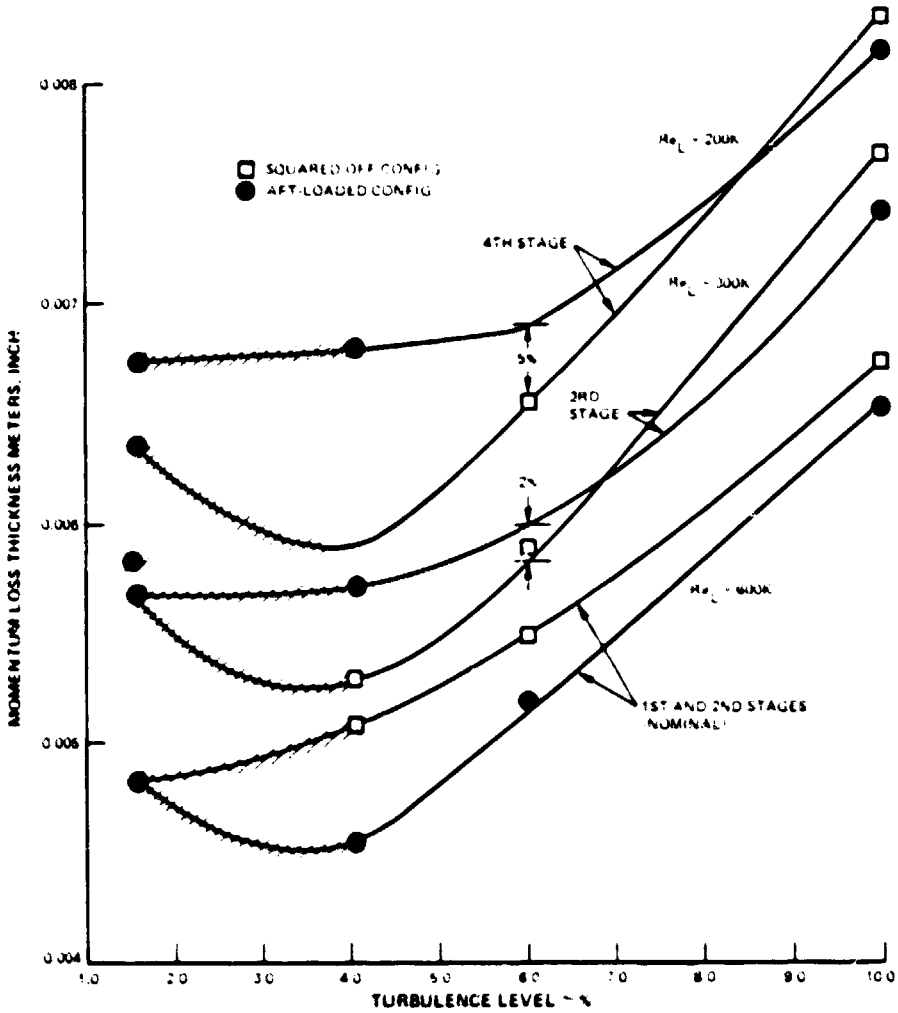

Figure 35 Boundary Layer Momentum Loss Thickness Calculation Results Obtained From the Analytical Study

Laminar separation was detected at the locations identified by the cross-hatched regions in the figure. The significant influence of Reynolds number and turbulence level on losses is apparent in this figure.

A decrease in loss with an increase in Reynolds number had been predicted for a fixed-inlet turbulence level for both airfoils. The influence of turbulence on losses was masked where laminar separation had been predicted on airfoil surfaces. Increases in turbulence level increased the loss at a fixed Reynolds number, if the results obtained with separation are ignored.

7.3 APPLICATION OF ANALYTICAL STUDY TO THE ENERGY EFFICIENT ENGINE

The program analytical study made it apparent that a knowledge of magnitude of turbulence in low-pressure turbines is important for estimating losses associated with boundary layers on airfoils. Although measurements of turbulence levels in full-scale turbines are not available, the levels are believed to be higher than those used in the experimental portion of the present program.

In the light of these problems, one has to rely on design experience. Turbulence intensity of the order of four to six percent is normally assumed for calculating profile losses. At a level of six percent turbulence, Figure 35 indicates that the squared-off pressure distribution would generate lower losses in the third and fourth stages of the low-pressure turbine and that the aft-loaded distribution would generate lower losses in the first and second stages.

Although the squared-off pressure distribution could reduce the fourth stage airfoil profile loss due to suction-surface boundary layers by five percent which would imply about a four percent lower profile loss for this distribution relative to the aft-loaded distribution--this benefit would decrease to two percent for the third stage.

One must exercise caution when applying these results to turbine designs. The analytical study was conducted in an environment removed from most experimental studies and can at best be used as an approximate guide by airfoil designers. Profile loss in a real engine is sensitive to many factors, such as unsteadiness, radial pressure gradients, and leading edge geometries, which were not accounted for in the two-dimensional, steady boundary layer calculations used in this study. These results highlight the need for validating turbulence models and increasing the data base to include an environment consisting of low Reynolds number and high turbulence intensities.

SECTION 8.0

CONCLUSIONS

This experimental and analytical investigation was conducted to assess the influence of the shape of free-stream velocity distribution on the development of two-dimensional boundary layers. This investigation has provided benchmark quality data that may be used to evaluate existing or new turbulence models for transitional boundary layers. A reliable turbulence model can be used in turn to optimize the shape of the free-stream velocity distribition on turbomachinery airfoils. The following specific conclusions can be drawn as a result of the present investigation:

- Experimental testing conducted at a relatively low turbulence level of 2.4 percent indicates that the squared-off distribution generates about 9 percent lower momentum loss thickness at the exit plane than the aft-loaded distribution.

- The results of the analytical study indicate that at high Reynolds numbers (typical of high-pressure turbines and early stages of low-pressure turbines) and high turbulence levels, aft-loaded pressure distributions have lower losses than squared-off pressure distributions. At low Reynolds numbers and high turbulence levels the trend is reversed.

- The overall results of the experimental and analytical program suggest that aft-loaded airfoils would result in better performance of the high pressure turbine and earlier stages of the low pressure turbine, whereas the squared-off airfoils would give better performance for the latter stages of the low pressure turbine.

- The McDonald-Fish turbulence model gives reasonable predictions for mean integral parameters in attached transitional boundary layers.

- Turbulence intensity profiles have a maximum at $y^+ = 25$ in laminar boundary layers. This maximum intensity increases in the streamwise direction, and the onset of transition occurs when the streamwise turbulence intensity $(\sqrt{u^2})$ reaches a threshold value of $3v^*$.

- Deductions, based on the present data and the work of Leipmann[8] indicate that the ratio of Reynolds-shear-stress to turbulence-intensity $(-\overline{uv}/q^2)$ is approximately the same for laminar and turbulent flow. The correlation coefficient $(-\overline{uv}/\overline{u^2}\ \overline{v^2})$ is also similar in these two flow regimes.

- Wall intermittency factor data in adverse pressure gradient boundary layers agree with the zero pressure gradient correlation of Dhawan and Narasimha. Thus, the intermittency factor distribution in transitional boundary layers is independent of the free-stream pressure gradient.

REFERENCES

1. Turner, A. B.: "Local Heat Transfer Measurements on a Gas Turbine Blade," Journal of Mechanical Engineering Science, Vol. 13, 1971.

2. Graziani, R. A.; Blair, M. F.; Taylor, J. R.; and Mayle, R. E.: "An Experimental Study of Endwall and Airfoil Surface Heat Transfer in a Large Scale Turbine Blade Cascade," Journal of Engineering for Power, Vol. 102, 1980.

3. McDonald, H. and Fish, R. W.: "Practical Calculations of Transitional Boundary Layers," International Journal of Heat and Mass Transfer, Vol. 16, No. 9, 1972.

4. Arnal, D. and Michel, R.: "Effect of Free Stream Turbulence on Turbulent Boundary Layers and on Boundary Layer Transition", EUROMECH 72, Boundary Layers and Turbulence in Internal Flows, University of Salford, Salford, U.K., March 30 - April 1, 1976.

5. Wilcox, D. C.: "A Model for Transitional Flows", AIAA Paper No. 77-126, 1977.

6. Donaldson, C. du P.: "A Computer Study of an Analytical Model of Boundary Layer Transition", AIAA Paper No. 68-38, 1968.

7. Forest, A. E.: "Engineering Predictions of Transitional Boundary Layers", Laminar-Turbulent Transition, AGARD-CP-224, Paper 22, 1977.

8. Dhawan, S. and Narasimha, R.: "Some Properties of Boundary Layer Flows during Transition from Laminar to Turbulent Motion", Journal of Fluid Mechanics, Vol. 3, pp. 418-436, 1958.

9. Emmons, H. W.: "The Laminar Turbulent Transition in a Boundary Layer - Part I", Journal of Aero Science, 1951, pp. 490-498. Also, Emmons, H. W. and Bryson, A. E., "The Laminar Turbulent Transition in a Boundary Layer", Proceedings of the First National Congress of Theoretical and Applied Mechanics, pp. 859-868, 1951.

10. Schubauer, G. B. and Klebanoff, P. S.: "Contributions on the Mechanics of Boundary Layer Transition", NACA TR 1289, 1956.

11. Cales, D.: "The Law of the Wake in Turbulent Boundary Layer", Journal of Fluid Mechanics, Vol. 1, 1956. Also, Coles, D.: "The Young Person's Guide to the Data", A Survey Lecture Prepared for the 1968 AFOSR-ISP-Stanford Conference on Computation of Turbulent Boundary Layers.

12. Liepmann, H. W.: "Investigations of Laminar Boundary Layer Stability and Transition on Curved Boundaries", NACA ACR No. 3H30, 1943. Also "Investigation of Boundary Layer Transition on Concave Walls", NACA ACR No. 4J28, 1945.

13. Bammert, K. and Sandstede, H., "Measurements of The Boundary Layer Development Along a Turbine Blade with Rough Surfaces", ASME Paper No. 80-GT-40, 1980.

14. Owen, F. K., "Transition Experiments on a Flat Plate at Subsonic and Supersonic Speeds", AIAA Journal, Vol. 8, No. 3, pp. 518-523, 1970.

15. Sharma, O. P.: "Coriolis and Curvature Effects in Boundary Layers of Centrifugal Impellers", PhD Thesis, Department of Mechanical Engineering, University of Birmingham, Birmingham-15, U.K., May 1975.

16. Dunham, J.: "Prediction of Boundary Layer Transition on Turbomachinery Blades", Technical Paper I-3, AGARD-AG0164, December 1972.

17. Patankar, S. V. and Spalding, D. B.: "Heat and Mass Transfer in Boundary Layers", Intertext Books, London, 1970. Also, Crawford, M. E. and Kays, W. M.: "STAN-5 - A Program for Numerical Computation of Two-Dimensional Internal and External Boundary Layer Flows", NASA CR-2742, 1976.

18. Ludweig, H. and Tillmann, W.: "Investigation of the Wall Shearing Stress in Turbulent Boundary Layers", NACA Report TM 1285, 1949.

19. Klebanoff, P. S.: "Characteristics of Turbulence in a Boundary Layer with Zero Pressure Gradient", NACA Report 1247, 1955.

LIST OF ABBREVIATIONS

B	constant for the law-of-the-wall
C	correlation coefficient, $-\overline{uv}/\sqrt{\overline{u^2}}\ \sqrt{\overline{v^2}}$
C_f	skin frictrion, $2\ \tau_w/\rho U^2_\infty$
C_p	pressure coefficient
E	mean voltage, instrumentation signal
e	fluctuating voltage, instrumentation signal
e^2	voltage, turbulence intensity signal
L	total test surface (or airfoil suction surface) length
H	shape factor, δ^*/θ
k	Von Karman's constant
P	static pressure
P_T	total pressure
$\overline{q^2}$	turbulence energy, $\overline{u^2} + \overline{v^2} + \overline{w^2}$
Re_L	Reynolds number, $U_{exit}\ L/\nu$
Re_θ	Reynolds number, $U_\infty\ \theta\ /\nu$, Boundary Layer Momentum Loss Thickness
s	surface or streamwise distance
s_t	location at the end of transition region
s_T	location at the onset of transition region
Tu	inlet turbulence level, $\sqrt{\overline{u^2}}/U_{inlet}$
U	streamwise component of mean velocity
U^+	dimensionless velocity, U/v*
U	velocity at edge of boundary layer
u	fluctuating streamwise component of velocity
u^+	dimensionless turbulence intensity, $\sqrt{\overline{u^2}}/v^*$

$\overline{u^2}$ streamwise component of turbulence intensity

$\overline{-uv}$ Reynolds shear stress

V mean velocity perpendicular to test wall

v fluctuating velocity perpendicular to test wall

v^* friction velocity, $= \sqrt{\tau w/\rho}$

$\overline{v^2}$ normal component of turbulence intensity

$\overline{w^2}$ traverse component of turbulence intensity

y normal distance from wall

y^+ dimensionless distance from wall, $y\ v^*/\nu$

γ intermitancy factor

λ measure of transition length

τw wall shear stress

δ boundary layer thickness

δ^* boundary layer displacement thickness,

$$\int_0^{\delta} (1 - U/U_\infty)\, dy$$

θ boundary layer momentum loss thickness,

$$\int_0^{\delta} \frac{U}{U_\infty} (1 - U/U_\infty)\, dy$$

ν kinematic viscosity

ρ density

REF Reference condition taken at the exit plane of the test section

APPENDIX A

TEST SECTION COORDINATES

The coordinates for the aft-loaded and squared-off test section configurations are:

AFT-LOADED CONFIGURATION (Figure 36)		SQUARED-OFF CONFIGURATION (Figure 37)	
s mm	H(s) mm	s	H(s)
0.0	203.2	0.0	203.2
75.784	143.51	69.6	142.75
94.234	132.08	78.74	136.14
113.284	123.19	96.77	124.46
131.825	116.586	114.55	114.55
150.114	112.27	131.83	106.43
168.148	109.22	148.59	99.57
191.0	106.172	165.1	93.73
210.0	102.4	184.15	87.12
246.9	98.55	210.31	78.49
274.3	95.0	235.97	79.25
302	91.7	262.38	84.07
330	88.9	289.56	86.61
358.65	86.6	318.26	86.69
387.9	84.33	347.73	86.87
417.83	82.04	378.21	85.34
448.31	79.0	409.2	83.57
463.8	77.22	440.9	83.31
479.3	75.18	473.2	85.09
495.05	73.15	505.71	86.87
511.0	75.96	538.7	88.65
527.05	77.72	571.76	88.65
561.1	83.82	605.03	91.69
592.33	87.38	638.6	93.22
626.11	89.66	672.34	94.74
693.17	95.25	706.12	96.27
727.2	97.79	739.9	98.04
761.5	100.08	773.94	100.08
795.8	102.11	807.97	102.62
914.4	107.2	914.4	111.51
1524	107.2	1524	111.51
2438.4	203.2	2838.4	203.2

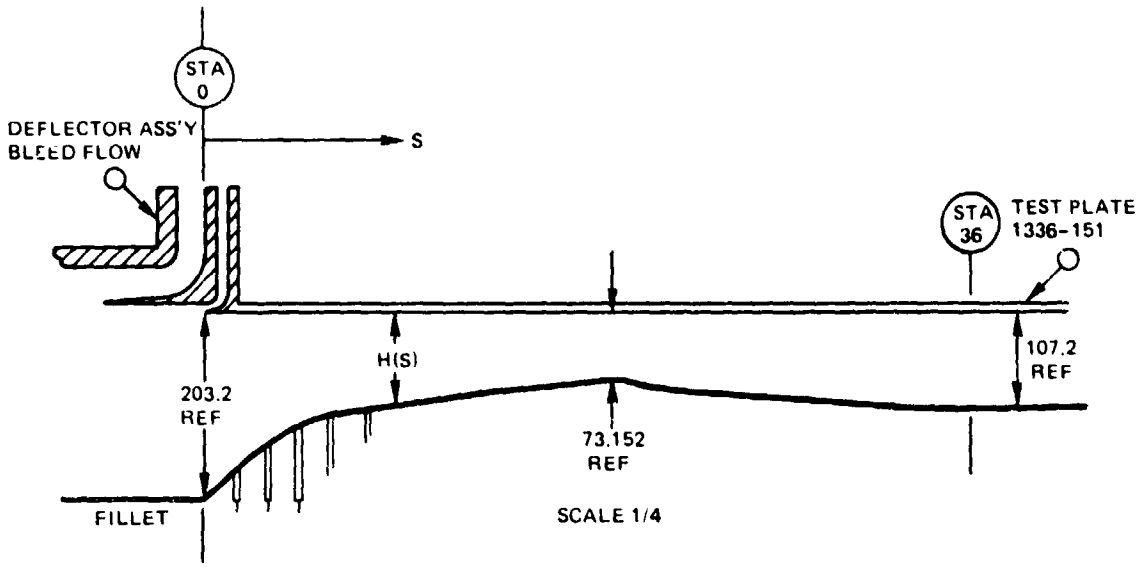

1. CONTOUR WALL SHOULD BE SMOOTH
2. CONSTANT DUCT HEIGHT 107.2 MM FROM STA. 915 TO STA. 1524
3. SIX DEGREE HALF ANGLE DIFFUSION FROM STA. 1524 TO STA. 2438

Figure 36 Schematic of the Aft-loaded Test Section

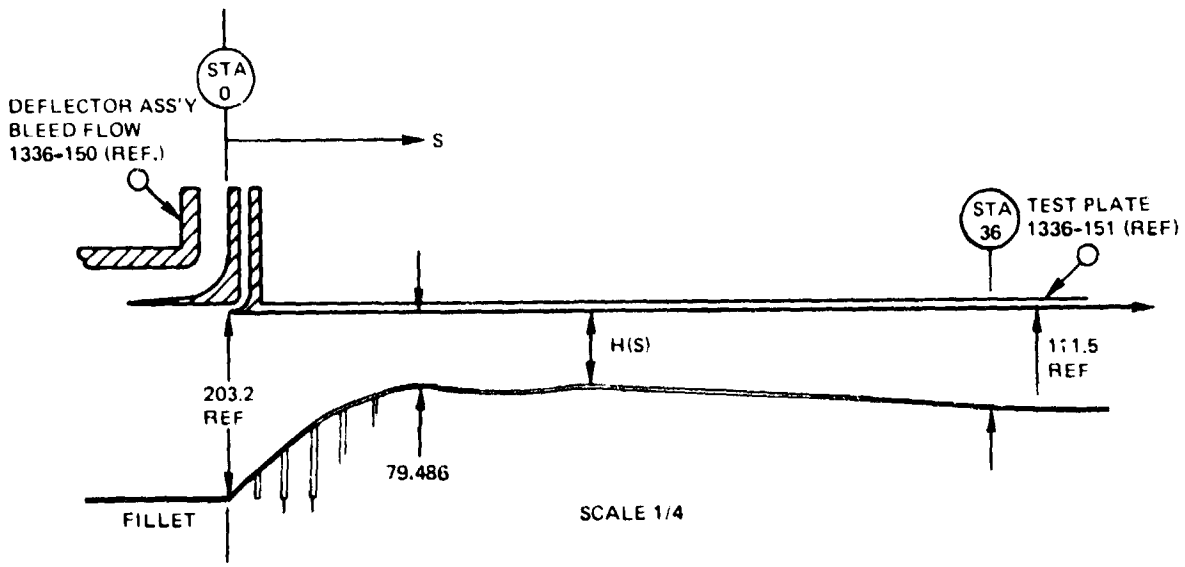

1. CONTOUR WALL SHOULD BE SMOOTH
2. CONSTANT DUCT HEIGHT 107.2 MM FROM STA. 915 TO STA. 1524
3. SIX DEGREE HALF ANGLE DIFFUSION FROM STA. 1524 TO STA. 2438

Figure 37 Schematic of the Squared-off Test Section